Intense shock waves and extreme states of matter

E. N. Avrorin, B. K. Vodolaga, V. A. Simonenko, and V. E. Fortov

Russian Scientific-Research Center 'Chelyabinsk-70';
Scientific Research Center of Intense Impulse Loading Studies, Russian Academy of Sciences, Moscow
(Submitted 18 December 1982; resubmitted after revision 28 January 1993)
Usp. Fiz. Nauk. **163**, 1–34 (May 1993)

A review is given of recent advances in the physical properties of matter that arise at ultrahigh pressures when solids are compressed and irreversibly heated by intense shock and rarefaction waves. Experiments have been carried in the proximity of a nuclear explosion, and also with chemical explosives employing geometric and gradient cumulation. High-speed diagnostic techniques and interpretations of dynamic experiments are described. Measurements of shock compressibility under pressures of tens, hundreds, and thousands of millions of atmospheres are presented. Part I analyzes theoretical models of highly compressed plasma and, in particular, the contribution of the discrete spectrum to its thermodynamics. A comparison is made with nonideal plasma models and the role of phase transitions and of quantum shell effects is analyzed. Part II discusses determinations of the velocity of rarefaction waves that provide information on the optical properties of hot condensed-state plasmas. Determinations of the thermodynamic and radiative properties of plasmas produced by adiabatic expansion of shock-compressed states have led to advances in the theoretically difficult near-critical region of metals in which strongly coupled plasmas are produced and there is a change in plasma statistics.

Dedicated to the memory of Academician Ya. B. Zel'dovich

INTRODUCTION

The advent of intense sources of highly directional forms of energy, such as laser beams, electron, ion, and neutron beams, shock and electromagnetic waves, and so on, has in turn led to laboratory studies and to technological applications of ultradense states of matter at previously unattainable extreme pressures and temperatures. Numerical simulations based on computer solutions of the equations of the mechanics of continuous compressible media in which different complicated physicochemical transformations take place at high temperatures and pressures have become an essential component of physical analyses and optimizations of impulse processes involving dense plasmas. Studies of these processes constitute an exceedingly difficult and interesting problem in the science of extreme states of matter.

The foundations of this science were laid by Academician Ya. B. Zel'dovich[1,2] with whom we were lucky enough to work and whom we will always see as our teacher.

The basic difficulty in the theoretical description of extreme states of matter is the presence of a strong mechanical interaction in the disordered medium, which means that perturbation theory cannot be applied to the corresponding quantum-mechanical many-body problem.[3] This in turn forces us to introduce physical models based on simplifying assumption about the structure, the energy spectrum, and the nature of the interaction between the constituent particles. These models are essentially extrapolations of collective and quantum effects in the thermodynamics of weakly-nonideal media and are therefore in acute need of experimental verification.

The significant point here is that several theoretical models predict highly nonmonotonic behavior of thermodynamic functions, due to thermal ionization and (or) ionization by pressure, deformation, and rearrangement of the energy spectrum of atoms and ions on compression, and also strong Coulomb interactions in plasmas. These phenomena can often lead to hypothetical phase transitions that can substantially distort the usual form of the phase diagram of metals and can complicate the qualitative description of time-dependent hydrodynamic phenomena.

The aim of this review is to examine experimental verifications of these intriguing predictions and to discuss factual information about the thermodynamics of condensed matter at extreme thermal-energy concentrations. Since a considerable number of specialist reviews and monographs is already available on this topic (see Refs. 1–11 and the references therein), we shall concentrate our attention on studies of ultrapowerful shockwaves and expansion adiabats of metals in shock-compressed and heated states, published during the last decade. In the final analysis, it was these studies that have resulted in a considerable expansion of the range of parameter values accessible to physical experimentation. They have also led to the exploration of an exceedingly wide portion of the phase diagram of metals, which now consist of seven orders of magnitude in pressure and five orders in density. Very different, complicated, and little known physical processes occur in plasmas in this region. They include multiple thermal ionization, deforma-

 1063-7869/93/050337-28$10.00

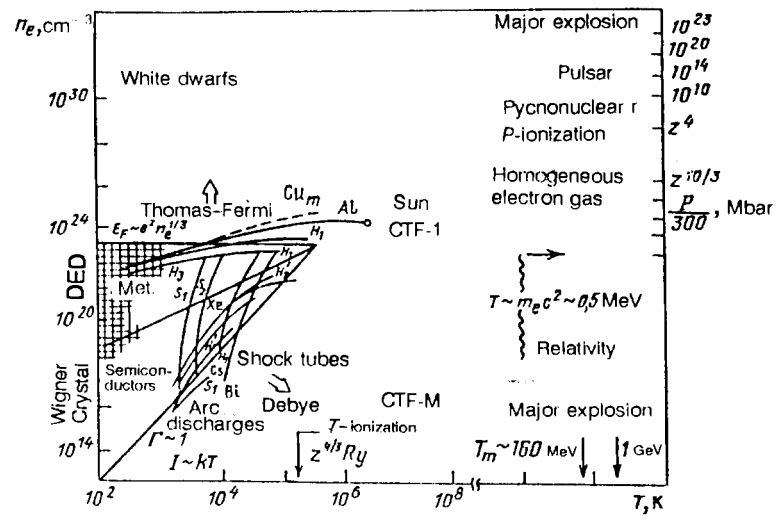

FIG. 1. Phase diagram of matter: S_1—adiabatic compression of saturated cesium vapor, $H_1', H_2; H_2', H_T$—compression of saturated cesium vapor and inert gases by incident and reflected shock waves; shock compression of continuous (H_3) and porous (H_m) metals; Al and Cu_m—shock adiabats of aluminum and porous copper, S_2—adiabatic expansion of shock compressed metals. Bi—expansion isentropes of bismuth.

tion of the energy spectrum of bound electrons ('shell effects'), the lifting of the degeneracy of electrons, the overcoming of the strong Coulomb interaction, the metal-dielectric transition, and high-temperature boiling.

In Sec. 1, we present the classification of plasma states and examine the corresponding thermodynamic trajectories and possible dynamic experiments. In Sec. 2, we consider the physical basis and limitations of modern theoretical models of the thermodynamics of extremal states. In Sec. 3, we discuss experimental techniques for the production and diagnostics of plasmas by compressive shock waves and adiabatic expansion waves, concentrating our attention on the correct interpretation of measurements. In Secs. 4 and 5 we analyze the absolute (Doppler shift and γ-standard) and relative methods of measuring the shock compressibility of metals at ultrahigh pressures from the point of view of identifying shell effects in the thermodynamics of hot plasmas. In Sec. 6, we present determinations of expansion isentropes of shock-compressed metals.

In the concluding Sec. 7, we discuss studies of the optical opacity of aluminium and iron.

1. GENERAL CHARACTERIZATION OF EXTREME STATES

Qualitative analysis of extreme states of the electron subsystem can be based on the consideration of Fig. 1 which summarizes the characteristic dimensionless parameters of plasmas, their technological applications,[3,8] and also the typical pressures (in the atomic system of units in which $P_a = e^2/a_B^4 \sim e^{10}m^4/\hbar^8 \sim 300$ Mbar) that are encountered in cosmic and nuclear objects. The relative strength of the interaction between particles in a Coulomb system is characterized by the dimensionless parameter $\Gamma = E_e/E_K$, i.e., the ratio of the mean Coulomb energy ($E_e = Ze^2/r_e$) to the kinetic energy (r_e is the screening length).

Below the $\Gamma \sim 1$ curve, the interaction in the classical plasma is weak and can be described by the chemical equilibrium model[8] with perturbation theory[12] used to calculate corrections for nonideal plasma behavior. Such calculations are, strictly speaking, asymptotic in character ($\Gamma \to 0$). However, dynamic experiments with cesium and inert-gas plasmas[3,8,12] show that several of the most successful descriptions allow extrapolations of these corrections to the region right up to $\Gamma \sim 1$.

The statistics of the electron component is determined by the degeneracy parameter $n_e\lambda_e^3$ where $\lambda_e = (h^2/2\pi m_e kT)^{1/2}$ is the thermal de Broglie wavelength. The characteristic scale for the kinetic energy E_K in such plasmas is the Fermi energy $E_F = e^2 n^{2/3}/2m_e$, so that the compression of plasmas beyond the quantum nonideality limit $E_F \sim e^2 n_e^{1/3}$ leads to a simplification of its thermodynamic properties as $\Gamma \to 0$. In real plasmas, the presence of positively charged nuclei results in the formation of many-electron atoms and ions which must be described quantum-mechanically.[8] One of the simplest models in this field is the Thomas–Fermi model[4,5] which is based on the quasiclassical approximation to the self-consistent field approximation and is valid for ultrahigh pressures $P \gtrsim P_a \sim 300$ Mbar. However, comparison of the results obtained in this way with the more accurate band models shows that there are considerable discrepancies for pressures $P \gtrsim P_a$ for which quasiclassical considerations suggest that the electron shells become 'crushed' and a quasiuniform electron-density distribution is produced. One of the basic problems in the study of superextreme states is the ellucidation of the thermodynamic role of shell effects and the determination of the range of validity of the quasiclassical description.

It is clear from Fig. 1 that, at present, only the periphery of the phase diagram is accessible to rigorous theoretical analysis. The nonideal region of extreme states is of the greater practical interest, but, at the same time, presents the greatest difficulties for the theory.

When we examine modern problems in the physics of high energy densities, we have to remember that it is difficult in thermodynamic descriptions to identify a particular domain of states. To do it, we need information about

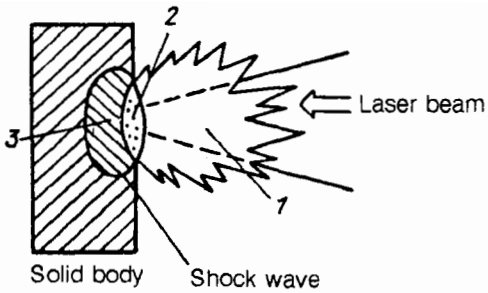

FIG. 2. Interaction of a laser beam with a solid target:[13] *1*—quasi-ideal plasma corona, $T \sim 1$ keV, $\rho < 10^{-2}$ g/cm^3, *2*—nonideal plasma, $T \sim 0.01$–1 keV, $\rho \approx 10$–50 g/cm^3, *3*—shock-compressed nonideal plasma; $T \sim 0.01-0.1$ keV, $\rho \sim 10$–50 g/cm^3.

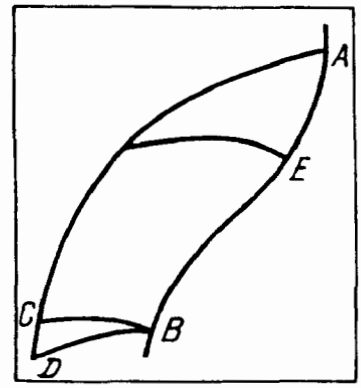

FIG. 3. Configuration of the region of states necessary for the simulation of the point-explosion problem.

the properties of matter in an exceedingly wide range of values on the phase diagram, beginning with a highly compressed condensed state and extending to the ideal gas theory, with the highly nonideal plasma in between. We shall discuss this by taking as an example the interaction between intense laser radiation and a condensed target (Fig. 2).[13,83] Let us suppose that the laser radiation is absorbed by the hot ideal-plasma corona *1* and that thermal energy is transferred to the region occupied by the relatively cold shock-compressed degenerate high-pressure plasma by electronic thermal conduction through the nonideal Boltzmann plasma *2*, encompassed by complex hydrodynamic motion. In controlled thermonuclear fusion with inertial confinement,[14] the target shown in Fig. 2 is the external ablator of a multilayer spherical thermonuclear microtarget that develops densities $\rho \sim 10^3$ g/cm^3 pressures $P \sim 10^5$ Mbar, and temperatures $T \sim 10$ keV. The effect of intense beams of relativistic electrons or ions is qualitatively similar to the situation illustrated in Fig. 2 except that most of the beam energy is now released in a region with high density $\rho \sim \rho_0$ (Refs. 14–16) and the expansion of the coronal plasma is nearly adiabatic.

To describe isentropic flow, we have to know the states along the corresponding line in thermodynamic space, i.e., the isentrope. In a more general case, when entropy is constant for each individual point, but is not constant for the entire flow, it takes the form of a surface determined by the equation of state in entropic form. The state of each particle then varies along the corresponding isentrope.

When shock waves are present in an adiabatic flow, the passage of a shock discontinuity across particular particles produces a discontinuous change in its state. The initial and final states lie on the corresponding shock adiabat of the material. The subsequent evolution of states occurs along the isentrope crossing the final point. A point explosion in a homogeneous medium is a typical example of this kind of flow, and the corresponding configuration is illustrated schematically in Fig. 3. The shock-wave amplitude decreases as it propagates outwardly from the center of the explosion, i.e., the point representing the state on the wave front moves along the shock adiabat AB. After crossing the front, the state of each particle evolves along the isentrope passing through the corresponding point on the shock adiabat. If, in a particular investigation, we are concerned with the parameters of the shock-wave front on which the intensity exceeds a particular value, e.g., $P_{fr} \gg P_E$, the domain of the necessary states lies above the characteristic drawn from the center to the point E. For the complete problem, the domain of states is bounded by the shock adiabat AB and the curve of states on the last characteristic.

If the motion in the medium is produced by the adiabatic expansion of a gas in a cavity (instead of a point explosion), the domain of states acquires a third boundary, i.e., the particle isentrope AC near the cavity, and the domain of states necessary for the simulation takes the form of the curvilinear triangle ABC. When we are concerned with the distribution of variables in flows of this type, the lower boundary of the domain of states is determined by the state of the profile at the last moment under consideration (the line BD) and the entire domain of necessary states is confined to the triangle ABD.

Let us now consider the compression of the homogeneous spherical microtargets used in controlled thermonuclear fusion with inertial plasma confinement.[14] When the intensity of the illuminating beams is not too high, the medium is compressed discontinuously on the front of the converging shock wave, followed by further isentropic compression behind the front. The domain of states lies to the right of the single compression adiabat and takes the form of a family of isentropes. The other boundaries of this region are determined by the properties of the compression regime. Thus, if the convergent flow is produced by the focusing of the shock wave, the amplitude increases (e.g., in accordance with the self-similar law[17]) as the center is approached. The character of the flow will change near the center as thermal conduction processes come into play,[18] after which radiation provides the dominant contribution to the increase in the energy density. Compression of matter near the center will not be adiabatic, and the particular state depend significantly on the loading conditions, the properties of the medium, and so on. The right-hand boundary of the domain for compression by a single wave is determined by states on the front of the shock wave

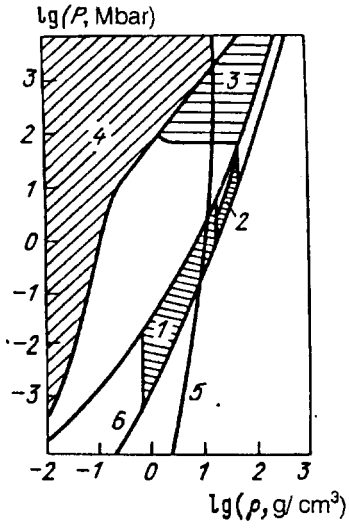

FIG. 4. Ranges of validity of different approaches to the construction of the equations of state: *1*—semiphenomenological models, *2*—continuous model, *3*—Thomas–Fermi model with corrections (TFC), *4*—ionization equilibrium model (Saha), *5*–shock adiabat, *6*–isotherm ($T=10^{-2}$ eV).

reflected by the center. When the target is illuminated by a profiled pulse, a centered compression wave can be produced within it.[19] In that case, the domain of states produced at the center of the target degenerates to an isentrope.

The state of matter in the outer layers of the target is due to processes associated with absorption of the incident energy. We have already mentioned that high temperature and low density of matter are typical for an evaporated particle. Some of the material adjacent to the evaporated particle successively passes through a series of states: prior to the arrival of the shock wave, the material at a given point is unloaded during the absorption of energy, e.g., the deceleration of fast electrons. The passage of the shock wave is followed by a transition to a shock adiabat that is different from the normal adiabat. Subsequent motion is isentropic.

The above examples clearly show that the equations of state must have a wide range of validity if they are to be used to simulate high-energy processes.

2. THEORETICAL MODELS OF EXTREME STATES

As noted above, no currently available thermodynamic theory of extreme states is capable of describing the entire phase diagram of matter. Moreover, because of fundamental difficulties encountered in a rigorous theoretical approach, the basic results can only be obtained by using models relying on simplifying assumptions about the structure, energy spectrum, and nature of the interaction between the particles. Naturally, the range of validity of such models is restricted by the nature of these approximations. In this Section, we confine our attention to the most typical theoretical models of extreme states and their comparison with experiment.

Figure 4 shows the phase diagram of alumnum with an indication of the approximate range of validity of the different theoretical models.

The perfect gas model is the simplest approximation used at low densities and moderate temperatures—lower by approximately an order of magnitude than the first ionization potential—for which thermal dissociation and ionization have not as yet taken place in the system and the interaction energy is low in comprarison with the particle kinetic energy. The most frequently used method of taking the interaction into account is the Mayer group expansion that leads to the virial equations of state. At high densities, commonly used procedures include the method of integral equations,[20] borrowed from the theory of simple liquids, and the Monte Carlo method[21] with perturbation theory for a spatially localized potential. This has recently increased the upper pressure limit to a few hundred kilobars, which is typical for the detonation of powerful condensed explosives.

A rise in temperature is at first accompanied by the dissociation of the outer (at $T\sim 1$–10 eV) and then inner (at $T\sim 10Z^{4/3}$ eV) electron shells of atoms. The ionization equilibrium in this type of system is described by the 'chemical' plasma model (the Saha model[8]) based on experimental and computed data on atomic and ionic excitation energies and also the corresponding ionization potentials. This model has an exceedingly wide range of validity that is limited at low densities and high pressures by the conditions for local thermodynamic equilibrium and stability ($T\lesssim m_ec^2\approx 0.5$ MeV) with respect to the spontaneous production of electron-positron pairs; at high energies it is limited by the low strength of the particle interaction, $\Gamma\ll 1$.

In early work, the Coulomb interaction was taken into account[22] by means of asymptotic expansions of arbitrary order in the expansion parameter and the diagram technique, which facilitated the regrouping and selective summation of the most divergent terms of the perturbation-theory series. The model consisting of a single-component plasma and a homogeneous neutralizing oppositely-charged background has recently been widely used to examine the role of collective and quantum effects in the Coulomb interaction. The model has now been investigated in detail by analytic and numerical Monte Carlo methods and by molecular dynamics.[24] Numerical results serve as 'standards', and improved approximate relations have been constructed for them and are used to establish the ranges of validity of asymptotic expansions. Such comparisons show that several modern analytic theories have good extrapolation properties up to $\Gamma\approx 2$, which can be improved further in accordance with the principle of local neutrality.[25] We note that very similar conditions for the validity of $\Gamma\approx 2$ theories also follow from comparisons with the results of dynamic experiments.[26,27]

It is important to note that computer simulations of highly-compressed single-component Boltzmann plasmas lead to thermodynamic anomalies and to the appearance of short-range order in the system. This is interpreted in Ref. 28 as the formation of an initial amorphous phase and then, at $\Gamma\approx 178$, of a crystal lattice. Phase anomalies of the

degenerate electron gas are discussed in detail in Ref. 29 where it is shown that, as this plasma expands, the formation of a charge-density wave is followed by the formation of the Wigner electron crystal.[40]

Special difficulties arise in compressed-plasma thermodynamics when an attempt is made to take into account the discrete spectrum of atoms and ions. In tenuous plasmas, configurations with closely-spaced particles have low probability, so that the continuous and discrete spectra can be separately taken into account by introducing atomic and ionic partition functions in different ways and under different limitations.[8] Such models lie at the basis of a large number of well-established engineering techniques[31] for the determination of the thermophysical characteristics of plasmas at moderate densities.

Shock-wave experiments with cesium, argon, and xenon plasmas,[6,8,26,27] and also experiments with shock-compressed liquid argon and xenon,[31] show that the particle interaction in highly compressed partially ionized plasmas produces a deformation and splitting of energy levels that cannot be described by perturbation theory and require a complete solution of the many-electron quantum-mechanical problem.

In the bounded-atom model,[37] internal atomic or ionic electrons are contained in a spherical cell of radius r_0 in which the electron-ion interaction potential has the Coulomb form

$$v_{ei}(r)=-\frac{Ze^2}{r}, \quad r<r_0, \quad =\infty, \quad r>r_0.$$

The radial wave function of each electron and the electron energy levels are calculated in this model by numerical integration of the Hartree–Fock equations with a nonlocal (exchange) potential. The resulting excitation energies are then used to calculate the partition functions for the chemical plasma model into which additional corrections are introduced for the Coulomb interaction, electron degeneracy, and the interaction between hard spheres of radius r_0, calculated from molecular dynamics. The variational principle $\partial F/\partial r_0=0$ then gives the equilibrium value of r_0. This is, of course, different from the value widely used in the cell model with dense packing.[33] In contrast cell models, 'the bounded atom' approximation is introduced within the framework of the quasichemical de-

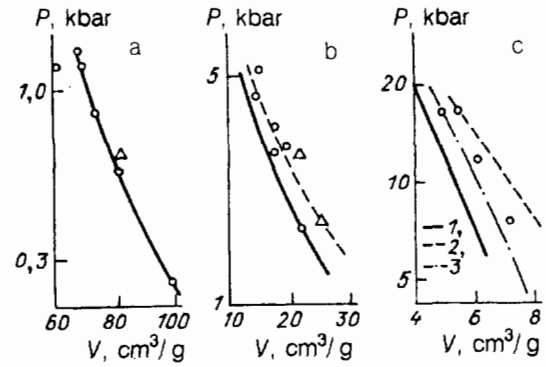

FIG. 5. Equation of state of argon plasma:[12] a–c—calculated adiabats from states with initial pressure of 1, 5, and 20 bar, respectively; *1*—Debye approximation in grand canonical ensemble, *2*—united atom model, *3*—pseudopotential model of plasma;[1,3,12] points—experiment.

scription in which the translational motion of the individual particles is explicitly taken into account together with the collective Coulomb interaction. Figure 5 compares this plasma model with shock-compression data for the nonideal cesium and argon plasmas. The same comparison will be made in Sec. 6 for superdense copper and aluminum plasmas.

The description of the bound states of electrons for condensed densities $\rho \gg \rho_0$ becomes very much simpler at extreme pressures $P \gg e^2/a_B^4 \sim 300$ Mbar and temperatures $T \gg \mathrm{Ry}=2\pi^2 me^4/ch^3=1.6\times 10^5$ K for which the electron shells become "crushed" and their properties are described by the quasiclassical approximation to the self-consistent field method, i.e., the Thomas–Fermi theory.[4,5] Among the large number of publications on this question, we note the generalization of the model to finite temperatures,[34] the detailed numerical investigationof the model in Ref. 35, and, especially, Refs. 36 and 37 which take into account correlation, quantum-mechanical, and relativistic effects. Because of the simplicity of both derivation and application, the statistical model has continued to be used to construct wide-range equations of state[12,38] and to obtain asymptotic estimates for thermodynamic functions.

Figure 6 shows the aluminum shock adiabats for different initial densities, calculated from the statistical

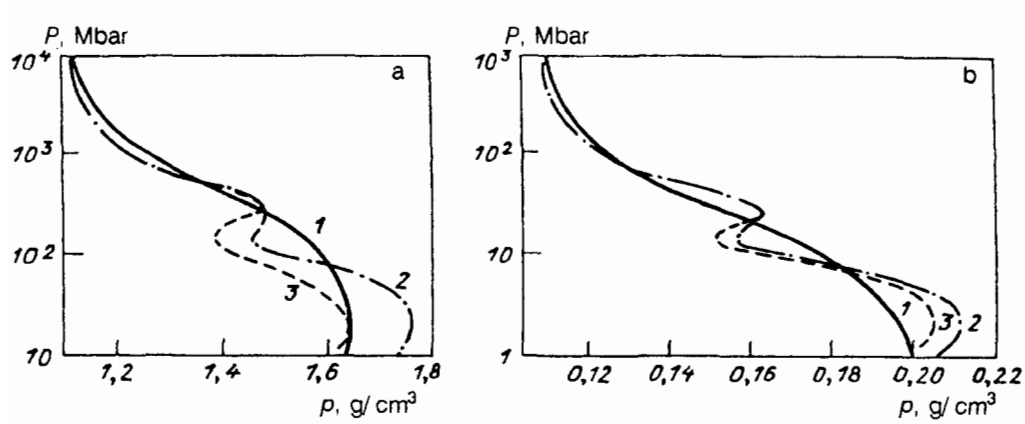

FIG. 6. Shock adiabats of aluminum with different densities: a—$\rho_{00}=0.271$ g/cm³, b—$\rho_{00}=0.0271$ g/cm³; *1*—TFQC, *2*—SCF, *3*—Saha.

model. As can be seen, there is good asymptotic agreement with the Saha model at ultrahigh pressures and temperatures.

The range of validity of the statistical description is related to the validity of the quasiclassical approach and the average description of a set of electrons in an atom, which ignores details of shell occupation and the associated nonmonotonic behavior of thermodynamic functions under compression. We emphasize that it was only during the last decade that shell effects, which arise naturally in plasma models,[1,8] have began to occupy the center of attention of theoreticians and experimentalists in the condensed state region. Careful analysis of quantum-mechanical effects[39,40] has shown that the quantum-dynamic model predicts oscillation effects, which have recently been taken into account[41] at finite temperatures. A more rigorous inclusion of shell effects necessarily takes us outside the framework of the quasiclassical model and involves quantum-mechanical self-consistent field approaches. The electron band theory was used in Ref. 42 with a number of simplifying assumptions to calculate the compression of simple materials at near-zero temperatures. It was found that the zero isotherms of certain elements displayed anomalous behavior. However, there was a substantial quantitative discrepancy between this theory and experimental data, which was probably due to the use of simplifying assumptions such as spherical atomic cells, the Hartree–Fock approximation, no correlation effects, and so on. So far, it has not been possible to extend the band model to high temperatures with the associated strong shock compression.

Subsequent publications[4,43–45,47] attempted to include shell-structure effects in the tranditional Thomas-Fermi model. Such modified models predict a wave-like or even discontinuous behavior for thermodynamic variables. Different models predict very different positions and amplitudes for the oscillations, which are often a consequence of internal defects of these models. For example, in the model employed in Ref. 47, the energy and pressure do not satisfy the thermodynamic identity and, judging by the fact that the energy is a function of compression at zero temperature, iron should have metastable states.

The model of Ref. 45 was improved in Ref. 48 and was augmented by simple broadening of levels into a band, i.e., its reflected a further fundamental property of compressed monatonic systems. The relative ease of calculations based on this model and the reasonable agreement with the results predicted by the more-advanced self-consistent field model[34,49] in the case of simple materials have meant that the model has been useful in calculations of the thermodynamic functions of mixture of atoms of different chemical elements.

The quasiclassical method of estimating shell effects has undoubtedly been successful, but a more rigorous inclusion of these effects can be based on the Hartree–Fock model (HF) in which the exchange interaction is taken into account in the Slater approximation (HFS). In the model employed in Ref. 50, the parameters of the Slater exchange potential were found from the condition for minimum free energy. An expression was obtained for the exchange potential in terms of the electron-density and temperature, i.e., the results reported in Ref. 51 were rigorously extended to arbitrary temperatures. This is reflected in the name of the model, i.e., the modified Hartree–Fock–Slater model (MHFS). The MHFS equations have also been obtained from the density functional.[52] The essence of this approximation is that instead of evaluating the multiparticle wave function for the electrons and then finding the electron density distribution function, the starting point is a chosen density functional whose form is determined by the adopted approximation. For the equilibrium electron density, the density functional (which is identical with the thermodynamic Gibbs potential) is a minimum. This means that MHFS a thermodynamically consistent model. The electron energy bands are found in this model (as in the band model) with the help of the Bloch boundary conditions. Subsequent approximations, which involve the inclusion of highly-excited electrons in the quasiclassical approxiamtion, produce a slight deterioration in the physical precision of the model. The limit of validity of the quasiclassical approximation is established individually for each material by what is essentially an empirical procedure.

An alternative model involving the self-consistent field (SCF) is proposed in Ref. 53 and constitutes a development of the model described in Ref. 47. The corresponding equations are obtained with the help of the density functional. As before, the lattice cell is spherical, and the pseudoband approximation is obtained with the Bloch boundary conditions. The following approximations are introduced and make the calculations very much simpler:

(1) the upper and lower band boundaries are found by the demanding that both the wave function and its derivative are zero on the cell boundary

(2) the electron distribution in each band is proportional to $(\varepsilon-\varepsilon_l)^{1/2}$ where ε_l is the lower boundary of the energy band

(3) electrons with energies $\varepsilon>\varepsilon_0$ are described quasiclassically.

The quantity ε_0 is essentially an empirical parameter that is chosen so as to achieve the best fit of the SCF to the experimental data at pressures at which SCF is known to be invalid. In contrast to Ref. 47, the SCF thermodynamic functions satisfy general thermodynamic relations.

The most complete calculations of thermodynamic functions of simple materials have been carried in the SCF and MHFS models. There are as yet no comparable data for chemically complex materials because of the difficulties in carrying out such calculations.

Improved descriptions of the electron component of matter require more accurate information on the properties of nuclei as compared with the widely used perfect-gas approximation that is invalid for dense media at temperatures $T\lesssim 100$ eV, which are important in applications.

The author of Ref. 54 has developed an approach in the equations of state of single-component plasma are calculated from the molecular dynamics of nonideal plasma. Inclusion of the thermal motion of nuclei in this modelel

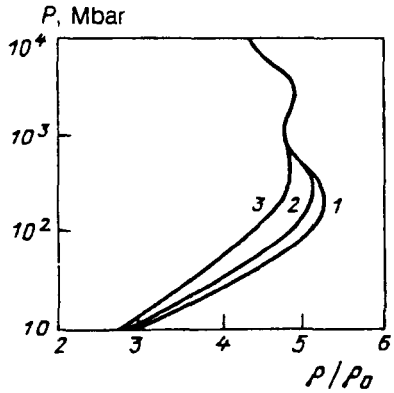

FIG. 7. Shock adiabats of aluminum obtained with different assumptions about the contribution of ions to the equation of state: *1*—ions described as a perfect gas, *2*—ions described by the approximation from Ref, 54, *3*—hard sphere approximation[55] for ions.

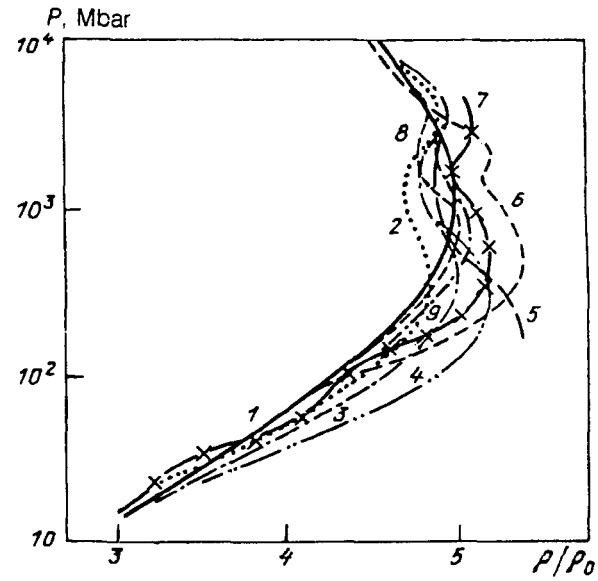

FIG. 8. Shock adiabats of aluminum obtained from different models: *1*—TFQC, *2*—SEOS (Ref. 28), *3*—SFC (Ref. 53), *4*—MHFS (Ref. 50), *5*—ACTEX (Ref. 58), *6*—INFERNO (Ref. 59), *7*—bounded-atom plasma model, *8*—density functional method (Ref. 131), *9*—quasi-ionic interpolation.[132]

has led, for example, to a shift of the shock adiabat to the left on the pressure—compression diagram (Fig. 7). It is found[132] that the correction for the inhomogeneity of the electron gas was taken into account twice in this model. Another defect of the approximation used in Ref. 54 is the assumption of point ions. The importance of the size of atoms and ions in highly compressed plasmas was analyzed in Refs. 12 and 27 in the light of direct experimental evidence for this effect, using the hard-sphere model with suitably chosen sphere dimensions. The same model was used in Ref. 55 to describe the strong interaction between ions at temperatures $T \sim 10$ eV and the radius of these spheres was calculated from the density distribution of bound atomic electrons, i.e., as a function of temperature, whilst the nuclear components of pressure and energy appear against the electron background. The reaction of the nuclear component on the electron component is neglected. According to Ref. 132, the hard-sphere model leads to a change in both the electron differential equations and in the use of consistent boundary conditions. Unless this is done, the corresponding model will be thermodynamically inconsistent to some extent. The approach adopted in Ref. 55 to the interaction of ions leads to steeper adiabats as compared with the preceding case (Fig. 7), but the role of thermodynamic inconstsencies has not as yet been identified.

The simplifying assumptions made in the SCF and MHFS models are as follows:

(1) thermodynamic functions are separated into the electron and nuclear components (the adiabatic approximation

(2) correlations between cells are ignored, i.e., the shells are assumed to be electrically neutral.

(3) the cells are spherical (there are difficulties with the description of the material before compression)

(4) the exchange interaction is given a simplified description (Slater 'local volume')

(5) energy bands are present in the low-density medium in which there is neither long-nor short-range order.

(6) the many-particle problem is replaced with the one-electron approximation

Even this simple listing of the simplifying assumptions indicates that these models require experimental verification and the identification of their ranges of validity. The effect of some of the simplifications on the measured thermodynamic functions is difficult to understand, but the differences introduced thereby are comparable with the magnitude of the total shell-structure effect. This is confirmed by the example of aluminum shock adiabats shown in Fig. 8. It is clear that there is an appreciable shell-structure effect even in the region in which the Thomas–Fermi approximation has been considered to be valid by optimists, whereas the maximum differences of oscillating shock adiabats from each other and from the smooth dependence are observed at pressures of 100 Mbar (for example, it is concluded in Ref. 56 that the Thomas–Fermi model was valid beginning with $P = 300$ Mbar at $T = 0$ and $P \sim 50$ Mbar at $T \sim 10^5$. Figure 8 also shows the shock adiabats obtained with the ACTEX and INFERNO models[57] in which the atomic shell structure is taken into account. ACTEX is based[58] on the equilibrium ionized plasma model in which the effective electron-ion potential is employed in a form determined from spectroscopic experimental data, and the ion-ion interaction is also taken into account. ACTEX calculations, performed within the range of validity of this model, lie between the data obtained by solving the Saha equations with and without Debye–Hückel corrections. In the region L-shell ionization, the electron-ion interaction becomes comparable with the kinetic energy on the aluminum shock adiabat, i.e., the lower oscillation wave is calculated outside the range of validity of the model. This explains why the ACTEX adi-

abat is as different as it is in this region. However, there is better agreement at high pressures (temperatures). Several of the approximations used in the MHFS and SCF models are the same as the approximations employed in INFERNO.[59] However, the levels do not split into bands in Ref. 59, and this affects the lower part of the adiabat: the onset of shell-structure effects is shifted in INFERNO toward higher pressures and is less well defined as compared with models capable of describing the splitting. Moreover, the thermodynamic variables are connected in INFERNO by different model relations (three possibilities are described), in contrast to the strict relation between them in SCF and MHFS. It is difficult at present to explain the discrepancy between the INFERNO shock adiabat and the other adiabats at pressures above 1000 Mbar because we do not have complete information about the model.

The complete quantum-mechanical model of the equation of state consists of three components, namely, the electron equations, the nuclear equation, and the boundary conditions for the surface of the atomic cell, which take into account the influence of electrons and nuclei on neighboring cells. The three components must be mutually consistent. This has not been achieved in most modern models (the exceptions are the Thomas–Fermi and QII models[132]). The effect of mismatched thermodynamics on the shape of shock adiabats (see Fig. 8) is not as yet clear, but we cannot exclude the possibility that some of the discrepancies in the amplitudes and phases are due to this particular factor. The quasi-ionic interpolation method (QII) proposed in Ref. 132, is based on models of ionization and chemical equilibrium and the quantum-statistical model in the respective ranges of validity with interpolation between them.

The need for the verification of modern theoretical equations of state and the identification of their ranges of validity has in turn led to an urgent need for experimental data on dynamic compression of matter in this range of extreme pressures and temperatures. Shock-wave experiments are at present the only way of investigating the thermodynamic prperties of condensed matter at about 100 Mbar.

3. DYNAMIC METHODS IN THE THERMOPHYSICS OF EXTREME STATES

Theoretical information is at present incomplete. Moreover, its fragmentary and contradictory character in the region in which different models overlap means that experimental methods of studying the thermodynamics of extreme states become pre-eminent.[1,3,6] The necessary empirical data can be obtained both by static compression and by dynamic experiments relying on shock-wave processes.

Static high-pressure techniques derive from the work of Bridgman[60] who carried out his pioneering investigations at pressures of the order of 100 kbar in the 1940s. Since the advent of particularly durable diamond (brilliant cut) anvils, the upper limit of static experiments has recently been raised to $P \approx 5$ Mbar. Diamond is transparent to optical and x-ray radiation, so that optical absorption and reflection measurements, Raman and Brillouin scattering, and x-ray difraction studies can be carried out on compressed materials, 1–20 μm thick. The basic problems at these higher pressures are the strength of the diamond anvils and the difficulties encountered in measuring high pressures by examining the shift of ruby flouresence lines with reference to shock-wave calibrations. The important point for us is that most measurements have been carried out for the $T \approx 300$ K isotherms with typical compression uncertainty of 10–20% in the megabar range.

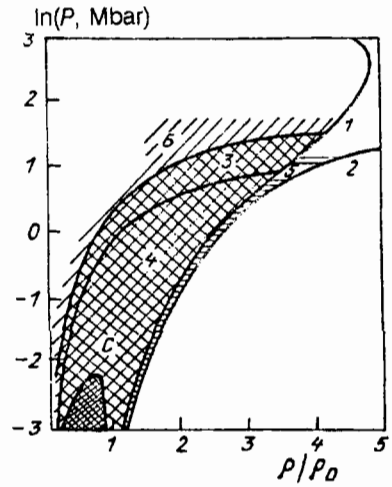

FIG. 9. Regions and characteristic lines accessible to experiment: *1*—single-compression shock adiabat, *2*—zero isotherm, *3*—isentrope, *4*—experiments on isoentropic rarefaction, *5*—region of two-fold shock and isentropic compression, *6*—experiments with media with different porosity; *C*—critical point.

The record static pressures of a few megabars were exceeded in the first dynamic experiment[6,62] in the 1940s as a result of the the higher energy densities typical of pulsed sources and the very substantial cummulation that was achieved in shock-wave processes.

Shock-wave experiments (see for example, Refs. 3, 6, and 9) involve measurements of shock compressibility under one- and two-fold compression of continuous and porous samples, the velocity of sound in the shock-compressed media, and the different optical and electrophysical parameters.[1,3,6–8]

Figure 9 illustrates typical states that can be produced in shock-wave experiments. For pressures $T \leqslant 5$ Mbar, the shock adiabat and the zero isotherms of dense condensed materials are not very different. States reached under shock-wave compression of solids are represented by the Hugoniot adiabat (curve *1*). Smaller temperature changes can be achieved by successively compressing a medium by two shock waves (liquid deuterium[63], aluminum[64]) or by using a magnetic field as a damping medium (plexiglass, hydrogen[65], silicon oxide[66]). The thermodynamic states reached in these cases (region *5* in Fig. 9) lie between the shock adiabat and the 'cold' compression curve ($T=0$ K; curve *2* in Fig. 9) which is close to the $T \approx 300$ K isotherm for which static measurements have been carried under $P \lesssim 5$ Mbar.

Higher temperatures and lower densities (as compared

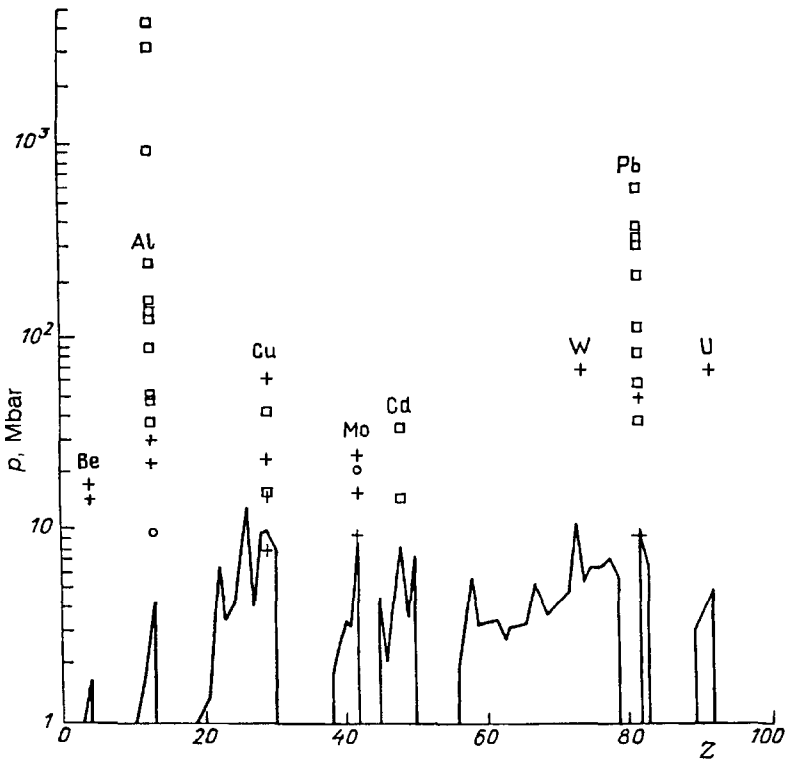

FIG. 10. Pressure ranges for experiments with powerful shock waves, in which shock compressibility of the elements has been measured in Ref. 73. Regions at the bottom (with sharp peaks)—experiments with explosives and guns;[3,6,7,9] underground nuclear explosions: circles—absolute measurements,[104,105] crosses—American data,[112-114,127] squares—Soviet data.[106,113,115,124]

with the shock-wave method) have become more interesting for the modern physics of extreme states.[3] These states can be reached by shock-wave compression of porous samples,[67-69] which sharply increases the irreversibility effect by increasing the shock-compression temperature and produces densities that are somewhat lower (by 20% in Ref. 68) than the density of a solid metal (states *6* in Fig. 9). A wider density range (up to 4 orders of magnitude) can be achieved by adiabatic expansion (states *4* in Fig. 9) after first shock-compressing and irreversibly heating the material under investigation.

A detailed discussion of these points is given in Sec. 6. We now turn to a consideration of the shock-compression method.

Shock-compression measurements rely on algebraic relations deduced from the conservation of mass, momentum, and energy. They relate kinematic parameters such as shockwave velocity D and mass velocity u behind the shock front to the thermodynamic variables such as the density $\rho=V^{-1}$, pressure P, and internal energy E (Ref. 1):

$$\rho=\rho_0 D(D-u)^{-1},$$
$$P=P_0+\rho_0 Du, \qquad (3.1)$$
$$E=E_0+\frac{1}{2}(P+P_0)\left(\frac{1}{\rho_0}-\frac{1}{\rho}\right),$$

where ρ_0, P_0, E_0 refer to the medium at rest and ρ, P, E to the medium behind the shock-wave front. Before we can apply (3.1) in a dynamic experiment, we must have a one-dimensional flow. This is usually produced by suitably choosing the geometry of the experiment, and is further monitored by direct measurement. The question of local thermodynamic equilibrium in shock-compressed states is usually not too acute because the ion-electron relaxation time in metals is indicated by theoretical estimates and laser-heating experiments to be about 10^{-11} s (Ref. 130), which is much shorter than the characteristic time of the experiments [about 10^{-6} s]. Moreover, (3.1) can be used for typical pressures in excess of the elastic yield point ($\sim$20 kbar) of the material,[10] so that the hydrodynamic approximation is valid.

When these conditions are satisfied, simultaneous measurement of D and u enables us to determine the thermodynamic variables E, P, ρ in a model-independent manner. This 'direct approach' has been used to investigate shock adiabats for a relatively small number of materials. In experiments performed in our country, iron has received more attention than other elements, and has subsequently been used as a standard in measurements of the 'relative' compressibility of materials by the 'reflection method'.[1]

There is now a very considerable volume of experimental data on shock compressibility. More than 200 materials have been examined. They include chemical elements, alloys, minerals, composites, organic and synthetic materials, liquids, gases, water solutions and condensed explosives. Existing experimental data on the thermodynamic properties of dense materials have been obtained in dynamic experiments and have been reviewed in the literature.[70,71] The amount of published information on shock compressibility obtained in dynamic studies is illustrated in Fig. 10, taken from Ref. 73. Measurements of shock compressibility are often accompanied by measurements of adiabatic compressibility (velocity of sound) be-

hind the shock-wave front, which involve an optical determination[72,74] of the velocity of the backward rarefaction wave that overtakes and attenuates the main shock wave. The loss of shear strength by a crystal lattice on melting leads to some reduction in the velocity of sound, and can be used to judge the position of the melting curve under high pressures.[75]

The first experiments on the excitation of shock waves in solids were performed with ballistic devices using the detonation of a condensed explosive to accelerate flat metal flyers to a velocity of 5–6 km/s (Ref. 5). Gradient acceleration[76] using the same geometry and a two-stage layered system has raised the velocity of a tantalum flyer to about ≈ 13 km/s, thus producing dynamic pressures of 4.2 Mbar in aluminium and 6.4 Mbar in bismuth.[77,78,87] Several experiments[79,80,87] have also been carried out with conically converging Mach shock waves at $P \sim 18$ Mbar. American scientists[81] have used a two-stage light-gas gun, capable of accelerating a 20-g impactor to a velocity of 8 km/s. This gun ensures the required timing of shock waves and accurate measurement of their parameters. Experiments with spherical converging shock waves[82] have produced steel flyer velocities of 8 km/s and pressures of 6.5 Mbar in uranium. In the experiments reported in Ref. 83, the flyer was accelerated to 20 km/s and the pressure in iron samples was about ≈ 13.5 Mbar. More recently, intense shock waves have been generated by powerful lasers,[83] high-current beams of relativistic electrons[15] and ions,[16] and rail-gun acclerators.[84,85]

The accuracy with which D and u could be measured in flyer-stopping method[1] deteriorates with increasing pressure and amounts to about 0.8–1% at 1–5 Mbar, 1–1.5% at 5–10 Mbar, and 1.7–2% at $\gtrsim 10$ Mbar. A different approach is necessary at higher pressures because, even in the most advanced form of the stopping method, the flyer cannot be accelerated without a rise in temperature. Two ways of measuring D and u at high pressures will be discussed later.

In most cases, the shock-wave velocity is measured in contacting media.[1] There is then no limitation on pressure, but the traditional interpretation of these experiments requires additional analysis. The procedure used to find the mass velocity in one of the two media relies on the relationships describing the shape of the hydrodynamic discontinuity on the boundary between the two continuous media (the method of P, u diagrams illustrated in Fig. 11) and on the assumption that a standard material with a known equations of state is available. It is assumed that the pressures and mass velocities are the same on the compact boundary. It is clear from Fig. 11 that the traditional procedure can be used to find the mass velocity if we know the shock adiabats for twofold compression and the unloading isentropes of the standard. The relationship between the uncertainties in the measured u_0 and D_e, D_0 is clear from Fig. 11. In view of what we have said about the accuracy of experimental data, the determination of the isentropes and twofold compression shock adiabats is based on model considerations whose validity and range of applicability must be verified in each case. The situation becomes much simpler only at low pressures ($P \sim 1$ Mbar) when the rise in temperature is small and the shock adiabats and isentropes are not very different from the 'cold' compression curve. On the P, u plane (See Fig. 11), the expansion isentrope AB (Fig. 11) is then the mirror image of the shock adiabat 1 of the standard relative to the point A. In this case, we must know the single-compression shock adiabat for the standard material, which can be obtained by the absolute method[1] in which a measurement is made of the velocity of a flyer and of the shock wave produced by it in a target.

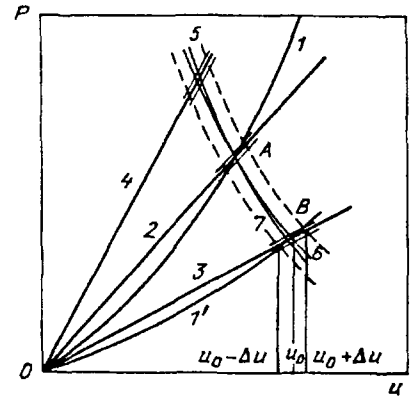

FIG. 11. Procedure used in the relative method to analyze experimental data: *1*—shock adiabat of standard material, *1'*—shock adiabat of barrier material, *2*—wave ray corresponding to measured $D_e+\Delta D$ and $D_e-\Delta D$, *3,4*—wave rays for samples, showing ray segments corresponding to $D_0+\Delta D$ and $D_0-\Delta D$; *5,6*—two-fold compression shock adiabat and isentrope of standard material, *7*—'mirror-reflected' shock adiabat of standard material. The diagram illustrates the determination of the mass velocity u_0 in the sample and the corresponding uncertainty.

We note that the replacement of the expansion adiabat with the mirror image of the shock adiabat in the megabar pressure range is also subject to considerable uncertainties due to the evaporation of the material in rarefaction waves (Ref. 3). At high pressures, the differences between the shock adiabat, the isentrope, and the twofold compression shock-adiabat become greater and the corresponding replacements give rise to substantial errors in the mass velocity determined in this way.

Experimental data are often analyzed in terms of the mirror-reflected shock adiabat.[6] In most cases, different reference materials are used in different pressure ranges, e.g., aluminum at low pressures and iron at high pressures. This must be borne in mind when shock compressibility data are systematically reviewed.

The following point emerged when an attempt was made to classify the data: experimental data on group four metals were obtained in the low-pressure region mostly relative to aluminum, whereas the data for iron were obtained at high pressures using aluminium as the standard material. In the pressure range that was investigated (potassium was among the metals), there was no detectable break on the D, u plane. We cannot exclude the possibility that such breaks may arise from the use in the analysis of the 'mirror-reflected' shock adiabats and from the fact that they may be different from the true shock adiabats of alu-

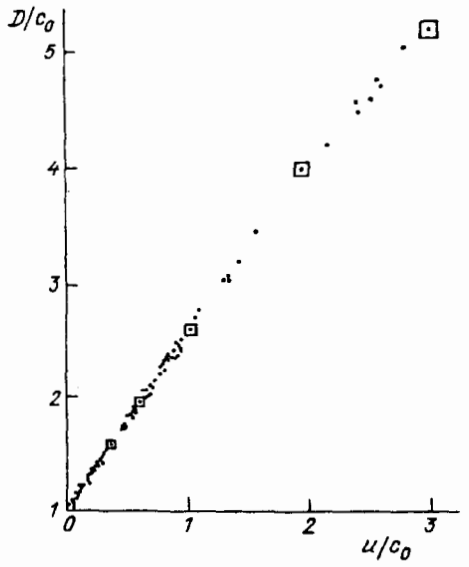

FIG. 12. Typical experimental D, u relation. the range of uncertainty corresponds to 1% precision in wave velocity.

minum and iron. It is interesting that some of the reported breaks have not been confirmed by subsequent experimental studies[88,89] and that for three of the materials the breaks are much less well defined and for mass velocities that are different from those reported in Ref. 86. We have therefore decided to repeat the analysis of all the results without using the 'mirror-reflected' shock adiabats.

The results of our analysis have led us to the following conclusions: the shock adiabats of metals on the D, u plane have a relatively complicated shape (Fig. 12) and can be approximated by linear or parabolic expressions but only within certain restricted ranges of pressure. Group four metals[86] are no different from other metals as far as their behavior on the D, u plane is concerned. This is illustrated by the results obtained for calcium and lanthanum (Fig. 13). To give an idea of the scale of experimental uncertainties, Fig. 13 shows rigorously calculated uncertainties corresponding to a 1% uncertainty in the measured wave velocity in the two media. Because of the methodological difficulties that arise in the analysis of experiments involving measurements of wave velocities in contacting media, a different approach to the interpretation of such measurements has recently been adopted. The entire analysis is performed in terms of directly measured D, D variables. The results calculated from models are also obtained in terms of these coordinates. However, this approach requires a greater volume of experimental data for the purposes of comparison and calibration because it is not clear which of the two media in the pair (and to what extent) is responsible for a possible discrepancy between theory and experiment. The model that is finally adopted is the one whose predictions in terms of the D, D coordinates are in agreement with experimental data for most pairs of media that are investigated.

We have collected and analyzed experimental data on the shock compressibility of several metals. In the pressure range typical for laboratory measurements, the approach adopted in Ref. 12, 90, and 91 is a good source of data for constructing semiempirical relations. A typical comparison between experimental and different models is shown in Fig. 14 in the case of the iron-lead pair. None of the theories can be rigorously justified in this pressure range. However, it is possible to find pairs of elements for which the experimental data can be described by one or other theoretical model for purely fortuitous reasons. For example, TFQC is in reasonable agreement with experiments involving iron and copper, but in most cases there is a substantial discrepancy between theory and experiment in this pressure range.

Experiments with powerful nuclear explosions provide data at higher pressures. For various reasons, the volume of experimental information obtained in this way is still limited and will not in the foreseeable future become comparable with the volume of data obtained in laboratory studies. It is therefore desirable to exploit the unique possibilities of such experiments to solve key problems in the physics of highly intensive processes.

We have already noted that studies of the effect of atomic shell structure on the thermodynamic properties of dense media have become increasingly important in recent years. Shell-structure effects are responsible for the oscillatory behavior of thermodynamic functions such as shock adiabats and isentropes. This in turn may give rise to the appearance of regions in which $(\partial^2 P/\partial V^2)_S \leqslant 0$ which is responsible for the anomalous behavior of matter in dy-

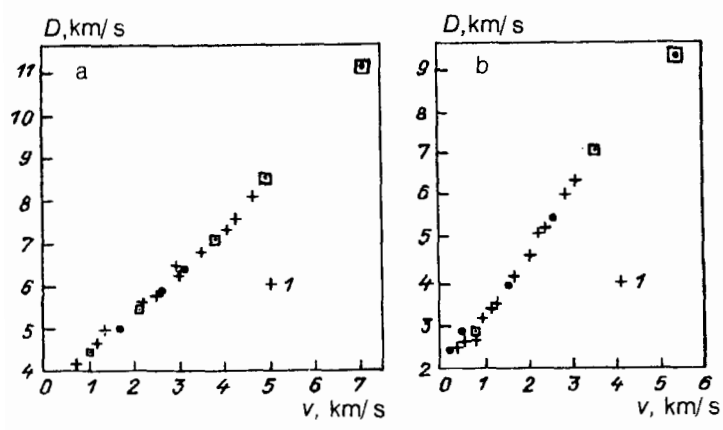

FIG. 13. Analysis[86] of experimental data for calcium (a) and lanthanum (b). The range of uncertainty corresponds to a 1% precision in wave velocity; *1*—data obtained by foreign authors.

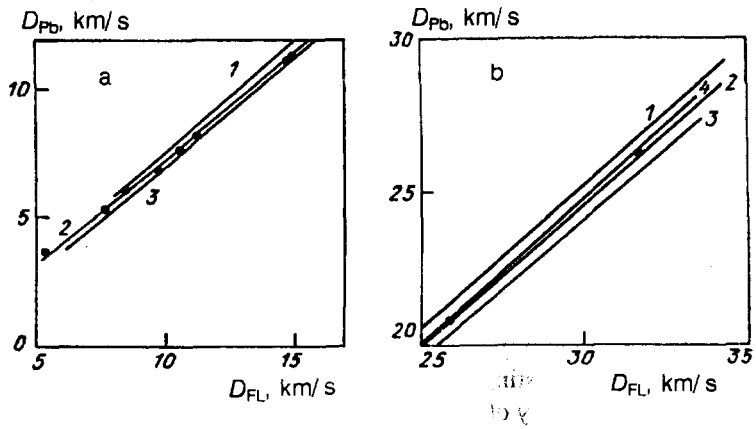

FIG. 14. Comparison of calculated D, D relations with experimental results: a—Ref. 86, b—Refs. 107 and 108, *1*—Ref. 38, *2*—Ref. 90, *3*—Ref. 91, *4*—TFQC.

namic processes (rarefactions occur in shock waves whereas compressionss occur continuously). The algorithms used in modern mathematical programs[92] must therefore be modified to take into account the properties of real materials in gas-dynamic calculations. This increases still further our interest in shell effects.

There are shock adiabats on which the stability conditions imposed on the curvature of shock fronts cease to be satisfied.[12,18]

Experimental uncertainties must be reduced as much as possible in regions in which there are conflicting theoretical predictions. To examine this problem, we turn to the model calculations[53,90] summarized in Table I.

If we adopt the MHFS model for the amplitude of the bottom half-wave of the oscillations, the numbers in the last row of Table I become greater by a factor of 2.

It is clear from these calculated results that shell-structure effects become detectable on the shock adiabats of aluminum when the wave and mass velocities are measured to within about $\approx 1\%$. The experimental uncertainties must be reduced to about $\approx 0.5\%$ if we wish to investigate the oscillations on the shock adiabat of lead or to verify particular models.

Similar precision is necessary when continuous samples are replaced with porous samples. This is indicated by calculations in which the porosity factor lay in the range 1–50, and also by experiments on shock compression of porous copper.[93]

Shock adiabats calculated from different models have frequently been published (e.g., for aluminum; cf. Fig. 8). The influence of different effects on the shock-wave velocity has recently been analyzed for a number of materials. As an example, we reproduce the results of measurements of D in a typical range.[124] The relative importance of quantum and exchange corrections was determined by calculations employing data from the TF and TFC models. The nonideal behavior of nuclei was examined in terms of the TFC and TFQC data (cf.[54]), shell effects were analyzed in terms of TFQC and SCF models, and the boundary conditions in terms of the SCF and MHFS models (Table II). It is clear that the corrections to the measured values of D are small and often have different signs. Powerful-explosion data (see, for example, Ref. 1) can be used to investigate the influence of a particular effect on the explosion energy determined from D, which is particularly important from the point of view of verification of nuclear tests. Estimates of shell effects can be based on the 'crust' approximation to the solution of the strong-explosion problem (see, for example, Ref. 1) and the description of the oscillating shock adiabat in terms of the pressure-compression variables relative to the limiting compression line $h=(\gamma+1)=(\gamma-1)$ in the form $\delta=h+\delta_1 \sin[K \ln(P/P_0)]$ where $\delta=\rho/\rho_0$, K and P_0 are interpolation constants, and, usually, $\delta_1 \ll \delta$. It can be shown by solving the problem that, when oscillations of this type are ignored, the uncertainty in the explosion energy is $\Delta E/E=[2\delta_1=h(h-1)]\sin[3K \ln(r/r_0)]$ where r_0 is the radial distance at which the pressure on the wavefront is P_0.

4. ABSOLUTE MEASUREMENTS OF SHOCK COMPRESSIBILITY

Dynamic methods of studying the equations of state are based[1] on determining two of the five shock-wave parameters E, P, V, D, u and calculating the remaining four parameters from the laws of conservation of mass, momentum, and energy (3.1). For condensed media, the most

TABLE I. Shock adiabat of aluminum.

D, km/s	40	60	80	100	120	140	160	180	200
P, Mbar	30,79	73,26	132,9	209,4	302,3	411,4	536,5	677,1	833,1
$\delta=\rho/\rho_0$	3,727	4,422	4,757	4,905	4,958	4,954	4,920	4,867	4,806
u_1, km/s	29,27	46,43	63,18	79,61	95,79	111,7	127,5	143,0	158,4
u_2, km/s	29,17	45,64	62,10	78,49	94,85	112,2	127,4	143,5	159,6
$(u_1-u_2)/u_1$, %	0,34	1,73	1,74	1,43	1,0	0,45	0,08	−0,35	−0,75

TABLE II.

Material	Quantum and exchange corrections	Nonideality of nuclei	Shell structure	Boundary conditions
Aluminum	+1,0	−0,1	−0,6	+0,2
	+1,8	−0,6	+1,0	+1,1
Iron	+1,4	−0,5	−2,4	
	+2,0	−1,5	−3,1	
Lead	+2,4	−0,6	+1,6	
	+3,3	−1,3	+1,2	

natural procedure is to determine the wave-front velocity D and the mass velocity u of the shock-compressed material. This was the approach adopted just after the last war. Recently, the attention of researchers has been focused on searches for ways of determining the distribution of the parameters of shock-compressed material, which can be done by using penetrating physical fields or by recording the temporal shape of the compression pulse rather than the mere fact of arrival of the pulse at the point of measurement. For example, when the shock-wave amplitude is small, so that there is little change in the properties of the media under investigation, the velocity u is measured by the magnetoelectric method that relies on the motion of a dielectric sample, containing a thin conductor, in an external magnetic field.[6,9]

Similarly, the electromagnetic method reported in Ref. 94 employs a sample containing one of the plates of a capacitor and measures the change in the electric field during subsequent motion.

At lower pressures ($\lesssim 100$ kbar), the mechanical properties of materials and the kinetics of detonation have been successfully studied with manganese pressure probes[9,95] whose resistance is a function of pressure.

At these relatively low pressures, the quasiacoustic approximation can be used to calculate the thermodynamic flow parameters from the velocity of the free surface of a sample after the arrival of a compression pulse. Capacitive methods[94] have been widely used for this purpose and laser interferometry has recently become available.[96,97]

Figure 15 shows the compression profile obtained in this way. It provides a variety of data on the strength, phase, and thermodynamic properties of matter.

Hard electromagnetic radiation can be used to obtain more extensive information about the situation behind a shock-wave front. For example, x-ray transmission of shock-compressed material[98,99] can be used to measure the density behind the shock-wave front or the velocity of opaque standard foils introduced into the medium under investigation. However, the precision of these methods is not high and they have not been widely used in studies of the thermodynamic properties of shock-loaded materials.

Interesting opportunities are offered by the x-ray diffractometry of shock-compressed materials,[98,99] which provides a direct way of determining the crystal-lattice parameters and of examining the course of the transition from one-dimensional to bulk compression behind the shock-wave front.

In particular, it is shown in Ref. 100 that the polymorphic transition of sodium chloride to the densely-packed structure is accompanied by the emergence of an intermediate phase.

The characteristic feature of dynamic methods is that, since they are based on measurements of the mechanical parameters and on the general conservation laws such as (3.1), they yield the equations of state only in the caloric form $E=E(P,V)$ which is thermodynamically incomplete because it does not contain the temperature or the entropy of the shock-compressed material. Under certain conditions, these quantities can be determined from $E=E(P,V)$ by using the first law of thermodynamics.[102] All this explains the considerable interest elicited by temperature measurements in dynamic experiments. Unfortunately, optical methods for the determination of temperature can only be used with optically transparent and isotropic media such as ionic crystals[101] or gaseous and liquid media.[3,102]

The range of dynamic studies can be extended further by using neutrons and γ-rays.

4.1. Doppler measurement of mass velocity

American researchers[104] have put forward a method of measuring mass velocities at high pressures, using the shift of resonances in the interaction between neutrons and nuclei in a moving material relative to the position of these

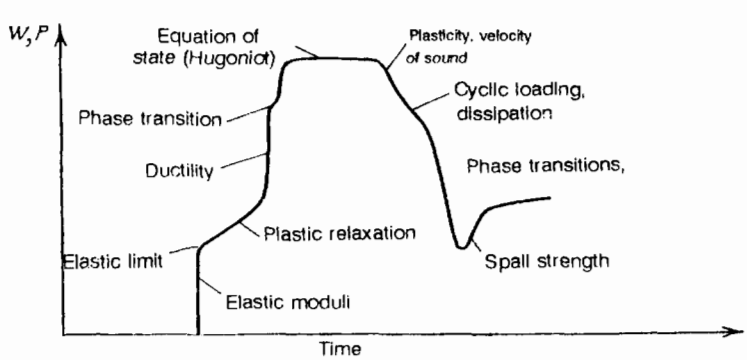

FIG. 15. Velocity and pressure profiles in a shock wave propagating in condensed media and the information that can be deduced from them.

resonances when the nuclei are at rest (Doppler shift). The energy released in the fission of uranium by neutrons from a nuclear explosion is used to produce the required high pressures. A plane foil of uranium is placed in contact with a sample of the material under investigation, which has a simple cubic structure. The shock velocity is determined by recording the instants of time at which light pulses are emitted by reference surfaces in the sample. The mass velocity is measured by using neutrons with energies in the range 10–10^3 eV, which usually contains nuclear resonances. The materials under investigation must have well-defined resonances so that a reasonable reduction in the neutron flux is achieved in the sample. When a resonance in the sample is observed at neutron energy E_n (or neutron velocity v_n) and some of the material in the sample travels in the direction in which the velocity u is measured, then there is an additional reduction in the flux of neutrons with velocity $v_n' = v_n + u$. The spectrum of neutrons transmitted by the sample will then have two peaks due to the particular resonance. The experimental problem is to record the neutron spectrum. If we suppose that the neutron source is instantaneous, the neutron spectrum can be determined from the neutron time of flight over a given baseline, say $L \sim 20$ m.

The neutrons in which we are interested transverse this baseline in a time $t \approx 5 \cdot 10^3$ μs. In Ref. 104, the length of a neutron pulse is 0.5–0.8 μs so that the pulse can be assumed to be instantaneous. The sample thickness is chosen so that a substantial proportion of it is moving during the operation of the source.

The neutron flux in the resonant energy range $E_n \approx 10$–10^3 eV is the significant quantity for the practical implementation of the method. The number of such neutrons in the fission spectrum is very small, but it was increased in Ref. 104 by inserting a thin layer of a hydrogen-containing material (Lucite) between uranium and the sample. The result was an increase in the neutron flux on the surface by approximately an order of magnitude.

This method of measuring the mass velocity is not universal. The cross sections at the resonances must be such that the reduction in the neutron flux due to both stationary and moving materials is readily detectable when the absorbing thickness is comparable with the measuring baseline. Such materials include molybdenum, iron, copper, and so on. There are also elements whose nuclei have an anomalously high resonance cross section (e.g., tungsten, gold, and cobalt). Mass velocity can be measured by inserting thin foils of such elements into the sample. Moreover, in some cases, the energy broadening of the individual resonances can be used to investigate the temperature of the medium on either side of the shock.

The resonances are particularly well-defined in molybdenum which was investigated in Ref. 104. A pressure of about 90 Mbar was produced in uranium and it was found that the velocities in this material were $D = 18.7$ km/s ($\pm 5\%$) and $u = 10.2$ km/s($\pm 5\%$) The precision of these measurements is not really high enough for the verification of the equations of state of molybdenum. The principal sources of error are the uncertainty in the duration of the

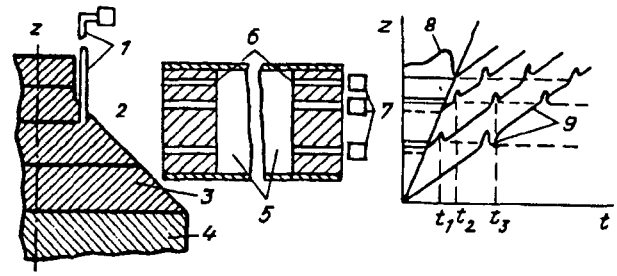

FIG. 16. Schematic of apparatus and tracings of recorded signals: *1*—optical channel, *2*—standard foils, *3*—material to be investigated, *4*—shock generation channel, *5*—collimating slits, *6*—collimator, *7*—γ-ray detectors, *8*—signal due to stationary standard, *9*—signal due to moving standard.

neutron pulse and the different types of resonance broadening. However, the contribution of many of these factors decreases with increasing mass velocity, so that $\Delta u/u \approx 1\%$ can be achieved, at least in principle, for $u \approx 100$ km/s. This will stimulate further explorations of this method.

4.2. The γ-standard method

The simultaneous determination of D and u by using γ-active standard foils, inserted into the material under investigation is reported in Ref. 105. These standard foils are dragged along by the medium during its gas-dynamic motion and a set of collimating slits is used to fix the instants of time at which the foils cross monitoring positions.

The planar geometry of the shock, the reference foils, and the collimating slits, for which all the relevant surfaces are parallel, is particularly convenient in practice (Fig. 16). A cylindrical channel made from a material such as magnesium, Lucite, and so on, whose density is lower than the density of the material in which the experimental setup is located is then placed along the path of the wave. Two-dimensional gas-dynamic calculations show that the channel ensures that the shock is well ahead of the shock in the ambient medium, and that the wave front inside the central portion of the cylinder (which is approximately two thirds of the outer diameter) is plane. The measuring unit is mounted at the end of the cylinder. The shielding of the collimating system, which prevents damage to it prior to the passage of the foils across monitoring positions, is accomplished by inserting foils of a dense material such as steel or lead into the path of the wave.

The mass velocity u is measured by recording the transit of a standard foil across two collimating slits separated by a distance a. The velocity is then given by $u = a/(t_3 - t_1)$ (see Fig. 16). The velocity D can be found by using two standard foils with two collimating slits and determining the corresponding times at the beginning of their motion: $D = a/(t_2 - t_1)$. The compression δ of the material on the wave front is a function of only the two time differences: $\delta = (t_3 - t_1)/(t_3 - t_2)$. The number of standard foils and collimating slits is usually greater than the aboove mini-

mum number. This provides information about the time dependence of the recorded shock-wave phenomenon and the course of neutron and γ processes.

The basic element used in the above simple time measurement scheme is the standard foil. The radiation emitted by it must pass through the peripheral layers of the material under investigation in which gas-dynamic motion is very different from the planar shock-wave flow. The standard foil should therefore contain sources of hard γ-rays or fast neutrons with energies $E_n > 1$ MeV. Since the relevant processes are time dependent and proceed at a high rate, the radiation intensity emitted by a foil must be high enough for secondary-emission and photoelectric analog detection as the foil passes the collimating slits.

Stationary sources of radiation cannot be used for these purposes. Even when highly sensitive detectors such as the photomultiplier (sensitivity $\alpha \sim 10^{-11}$ A $\cdot$ cm^2/photon) is employed, the source activity would have to be $\sim 10^7$ Ci. When the background is high, it is better to use FEK type detectors ($\alpha \sim 10^{17}$ A $\cdot$ cm^{2}s/photon). The necessary source activity is then much higher. Such sources are not available, but even if they were, it would be impossible to use them because their power output would have to be $\sim 10^4$ MW.

It follows that we have to use pulsed sources that become "live" on a particular stage of the gas-dynamic process that is being used. In particular, a strong γ-ray source can be produced by neutron bombardment of a material whose nuclei have a radiative capture cross section that is greater by a factor of about 10^3 than the corresponding cross section of the material under investigation. Existing pulsed sources usually produce fast neutrons with $E_n \sim 1$ MeV. Radiative capture reactions occur efficiently at lower energies, which means that the neutron pulse must lead the recorded gas-dynamic notion by the time interval necessary to slow down the neutrons in the medium under investigation down to optimum energy values. Standard foils can often incorporate europium for which the (n,γ) reaction cross section at energies $E_n = 10$–100 eV is $\sigma = 220$–80 b.

Aluminum is widely used as the standard material in applications of the reflection method. At energies of 5–150 Mbar, the equation of state of aluminum has significant ambiguities, which explains why aluminum was chosen for the first applications of the new method. Of course, there are other possible combinations of standard and sample materials. In some cases, pulsed neutron sources (convertors) can be used in the standard foils.

As the neutrons are being slowed down, diffusion and absorption have very little effect on their density. We can therefore estimate the necessary γ-standard activity $\Gamma(\mathrm{s}^{-1})$ in terms of the fast-neutron flux $\Phi(\mathrm{cm}^{-2})$ and the mass M of the standard material:

$$\Gamma \sim \Phi \sigma N v M l^{-1} \sim 0.2 \cdot 10^7 \Phi M; \qquad (4.1)$$

where σ is the cross section for the (n,γ) reaction on the nuclei of the standard material, N is the number of these nuclei per unit mass of the standard material, v is the velocity of the slowing-down neutrons, and l is the mean free path of the incident neutrons in the material under investigation. The numerical value reproduced here is for aluminum and Eu_2O_3, compacted to a density of 2.7 g/cm^3, as the standard material. Since, for europium, σ increases more rapidly than v^{-1} as the neutrons slow down, the intensity Γ will continue to increase until the rate at which neutrons enter the standard Al foils becomes equal to their rate of absorption by europium. Further slowing down of the neutrons is accompanied by a reduction in γ because the neutrons deplete the Al regions surrounding the standard foil. When the foil thickness is about 0.5 cm, the maximum radiation intensity is reached for $\sigma \sim 200$ b which corresponds to neutron energies $E_n \sim 10$–100 eV. The characteristic neutron slowing-down time from these energies is 10–15 μs.

The slowing-down of neutrons raises the temperature of the material under investigation which, in general, influences its shock compressibility. The interpretation of experimental results is simpler when this effect is small, which in turn imposes an upper limit on the flux Φ. For aluminum, acceptable values are $\Phi \leqslant 10^{17}$ cm^{-2}. The lower limit in (4.1) depends on the necessary increase in the size of the measuring unit.

Standard foils are effectively inhomogeneities in the medium under investigation. They are taken into account by gas-dynamic calculations when experimental results are analyzed. To reduce uncertainties associated with calculated corrections, the thickness of the standard foil should not exceed 10% of the measuring baseline. The apparatus used in the above experiments is capable of acceptable time resolution ($\Delta t/t \approx 1\%$) for time intervals of about 2 μs. This means that the shock compressibility of aluminum at a pressure of about 10 Mbar ($D \sim 25$ km/s) can be investigated with a baseline of 5 cm and a standard foil thickness $\Delta \lesssim 0.5$ cm.

The measuring unit (Fig. 16) is in the form a set of plates of AD-1 aluminum (99% Al, $\rho_0 = 2.7$ g/cm^3) with the standard foils inserted into it in the form of tablets. This foil shape is consistent with the cylindrical geometry of the channel in which the shock wave is produced, and allows the introduction of additional collimating systems. The maximum flux of recorded radiation in the direction of the detectors is produced by ensuring that the thickness of the material under investigation is as small as possible and does not distort the motion of the shock-wave front or of the material behind it in the region containing the standard tablets. The lateral surface of the unit on the side of the collimating system is therefore flat and at an angle of 45° to the direction of the shock front. The shape is monitored by three optical channels at the corners of an equilateral triangle, across a diameter of 150 mm (only one channel is shown in Fig. 16). The times at which light flashes appear when the shock emerges on a particular monitoring surface perpendicular to the axis of the unit are recorded.

The process of measurement is complicated by substantial background phenomena. The main sources of background are primary neutrons and also γ-rays created in (n,γ) reactions in the sample, in the different pieces of the apparatus, and in the ambient medium. The back-

ground neutron flux can be reduced by placing the detectors as far as possible from the medium under investigation. A collimating system is used to protect the detectors from capture γ-rays. Lead partitions can also entirely reduce the γ-ray flux originating in the apparatus and its environment. The only unattenuated radiation is then the one passing through the collimator slits. When FEK type detectors are employed, the length of the collimating system can be $L \sim 2$ m. The detector output current is related to the γ-ray intensity Γ from the standard foil by

$$I \approx \Gamma \alpha \exp(-\mu \rho d)(4\pi L^2)^{-1}, \tag{4.2}$$

where α is the detector sensitivity, μ is the mass attenuation coefficient for γ-rays in aluminum, ρ is the density of the compacted aluminum, and d is its thickness. To produce $I \sim 1$ A for $\rho \sim 10$ g/cm^3, $d \sim 10$ cm, and $L \sim 2$ m we must have $\Gamma \sim 10^{24}$ s^{-1}. According to (4.1), for $\Phi \sim 10^{16}$ cm^{-2}, the mass of the standard foil radiating toward the detector must be 50 g. The material of the standard foil is compressed behind the shock front by a factor of 3. The γ-rays that leave for the detector then originate from a depth of 2–3 cm in the standard material. The standard tablets used in the experiments have diameters of ~ 9 cm and thickness ~ 0.4 cm.

The collimating system is in the form of a set of coaxial and rigidly coupled lead discs with slots of 3×90 mm^2. The slot width is determined by the characteristic thickness to which the standard tablet is compressed by the shock (~ 1 mm) and the possible adjustment of the collimating system. The separation between the planes of the slots constitutes the measuring baseline. The precision with which these baselines can be determined depends on fabrication precision and on the extent to which the planes of the slit, the standard foil, and the shock front are parallel. The planes of the slits can be arranged to be parallel to the planes of the standard foils to within $\pm 0.2°$. The associated uncertainty in the baseline was negligible in comparison with the uncertainty in the system fabrication precision which was 2% for a baseline of 50 mm. Monitoring of the shape of the shock front was accurate enough to ensure that a correction could be introduced into the baseline for the departure from strict parallelism of the shock front and the standard foils.

To reduce the γ-ray background recorded by the detector prior to the arrival of the shock, the second and third standard foils (the numbering is in the direction of wave propagation) that are used to determine D are recessed by 1 mm relative to the planes of the corresponding slits (see Fig. 16). The fourth standard foil is placed at the center of the slit, and provides experimental information on the course of neutron and γ-ray processes.

The presence of strong sources of radiation in a sample gives rise to an increase in its temperature. When the shock arrives, it displaces the interface between aluminum and the standard and produces a change in the state of the two materials. This has a significant effect on the interpretation of experimental results and the corresponding process is taken into account by gas-dynamic calculations.

TABLE III. Absolute measurements on aluminum.

Ept. no.	ρ, g/cm^3	D, km/s	u, km/s	P, Mbar	$\delta = \rho/\rho_0$
1	2,55±0,03	24,8±0,5	15,7±0,3	9,9±0,3	2,73±0,08
	2,71	24,2±0,7	15,1±0,4	9,9±0,3	2,65±0,1
2	2,58±0,03	24,0±0,4	15,1±0,2	9,3±0,2	2,70±0,05
	2,71	23,4±0,6	14,5±0,3	9,3±0,2	2,63±0,07
3	2,71	40±5	30±2	32±2	3,9±1,2

The oscillograms are processed by widely available mathematical programs that take into account the attenuation of the signal along the transmitting cable, the properties of the recorded signal, possible sweep nonlinearity, and image distortion.

Apparatus built in accordance with the above principles has been used to perform three experiments on the shock compressibility of aluminum. Different versions of the apparatus differed from one another by the number of standard foils and collimating slits, the dimensions of the different parts of the apparatus, and so on.

The latest oscillogram-processing techniques, advances in dealing with time-dependent motion, and new standard foils are discussed in Ref. 106. The results obtained are summarized in Table III.

We recall that high intensity γ-rays from standard foils can increase the internal energy of aluminum up to about 1.5 kJ/g. The resulting pressure gives rise to a reduction in the density of the aluminum to about 2.55 g cm^3 and a compaction of the porous standard foil to a density of about 6 g/cm^3, i.e., the wave enters the sample in an initial state with $\rho_0 \approx 2.55$ g/cm^3 and $E_0 = 1.5$ kJ/g. The experimental points on the shock adiabat that starting from this initial state are listed in rows 1 and 3 of Table III. Rows 2 and 4 list values recalculated to the shock adiabat with $\rho_0 = 2.71$ g/cm^3 and $E_0 = 0$ under constant pressure. The recalculated values are not very dependent on model considerations.

In the third experiment, the measurements were carried out near the lower pressure limit for the appearance of shell effects. Unfortunately, we do not have fast enough oscillographs, so that the experimental results are subject to considerable uncertainties and cannot be used to test existing theories.

Our experience with the standard foil method of measuring shock compressibility shows that it is capable of considerable improvement in respect of different combinations of standard and tested materials and different experimental configurations.

5. RELATIVE MEASUREMENT OF SHOCK ADIABATS

The choice of the method used to determine the wave velocitie in compacting samples (the barrier method, 'relative' measurements[1,6]) depends on the pressure range. Specialists in underground nuclear explosions are familiar with techniques for producing shocks of different intensity and a prescribed shape of the shock front. The arrival of a shock on a monitoring surface is indicated by the closure of

electrical contacts, the emission light by air adjacent to the samples, and the emission of light by the vapor of the material in the rarefaction wave (see, for example, Refs. 107–111). The attentuation of a shock wave necessary for a transition from intermediate wave velocities to the values on the contact boundary is calculated and, usually, monitored experimentally. Corrections due to the heating of the medium ahead of the shock front, for example, by electrons in the case of experiments with laser pulses[83] or γ-rays (see Section 4.2), are determined by calculation. The precision of such measurements is determined by the properties of the recording equipment, by the characteristic of the transmission channel, by the attenuation of the wave inside the samples, and by the symmetry of the wave front relative to monitoring surfaces.

The fact that experimental data can be obtained throughout the pressure range that is of interest for applications has been demonstrated by Soviet and foreign researchers,[107–114] but these results could not be used in all cases to test theoretical models.

In the experiments reported in Refs. 107 and 108, the time intervals were measured with an uncertainty of 0.7–1.0%, and the attenuation of the wave was determined with an uncertainty of 1–2%, which meant that the wave velocity on the contact boundary was determined with satisfactory precision. These results can be used to test the validity of models, but they cannot provide answers to questions relating to shell structure effects; the measurements were carried out near the lower pressure limit for the appearance of shell effects. We recall that, in this pressure range, all models predict that shell effects should have litle influence on the behavior oif shock adiabats, and the D, D relations calculated from them are segments of straight lines with slopes that are not very model-dependent.

Approximately the same pressure range has been reached American experiments[112–114] in which molybdenum was usually the first material encountered by the shock waves. The wave velocities were determined to within 1.4–2.6%, depending on the sample, and corrections for attenuation did not exceed 2%. In addition, corrections were also introduced for the curvature of the shock front at the equipmental assembly with plane-parallel monitoring surfaces. The measurements were interpreted in terms of P, u diagrams. Analysis of the experimental in terms of the D, D coordinates provides additional information. In particular, we note the relation between the calculations and the data in Refs. 112 and 113. The measured velocities lie on opposite sides of the relations deduced from TFQC, so that the difference between them is smaller by a factor of 2 than the calculated difference. If this is a manifestation of shell structure, the position of the oscillations on the shock adiabats of lead and uranium cannot be explained by any existing model and is in conflict with experiment.[115] both in relation to amplitude and position. We note that the amount and precision of the molybdenum data reported in Ref. 113 and 114 are not sufficient to allow us to determine with the necessary precision the slope of the relationships on the D, D plane for the molybdenum-aluminum and melybdenum-iron pairs. The true velocities are likely to lie within the stated ranges of uncertainty and differ from the nominal experimental values because the slopes obtained for these pairs of lines joining the experimental points are appreciably different from the calculated values. There are no obvious physical reasons for this in the pressure range under investigation. Nuclear explosions and light-gas guns were used by American scientist[126] in recent studies to determine the shock compressibility of several metals in the pressure range 4–24 Mbar. The 'standard material' was aluminum whose dynamic properties were described by a theoretical equation of state.

Novel ideas for experiments at pressures near 100 Mbar have now been successfully tested.[109] However, the precision of the experimental results was not as good as expected. The main contribution to the experimental uncertainties was the uncertainty in the correction for the attenuation of the wave inside the experimental assembly, which has meant that the results obtained could not be used to test theoretical models. The change from the planar system of Ref. 109 to the spherical system employed in the measurements reported in Ref. 110 has produced still higher pressures. However, this change has been accompanied by a considerable attentuation of the shock wave in the samples, and the uncertainty in the correction for this has again provided the main contribution to the resultant uncertainty in these measurements.

In the nontraditional experimental studies of shell-structure effects reported in Ref. 111, the measured time taken by a shock to traverse different samples was compared with model calculations. The pressure at the shock front was found to fall by a factor of three or four in the sample, i.e., when the propagation of the wave is modelled, it is important to know not only the particular segment of the shock adiabat, but also the segment of the rarefaction isentrope (see Fig. 3). It is therefore unclear whether this type of measurement can be unambiguously interpreted. In a particular case,[111] the experimental uncertainty was found to be to high for the experimental detection of oscillations.

Ways of reaching the required precision were found as a result of an analysis of the experimental data reported in Ref. 109 and 110. Well-defined shock-front shapes were produced in special assemblies, and standardized measurements were performed for several values of the pressure at the wave front. The measurement baselines were chosen so that the behavior of the wave velocities in the foils under investigation was shown by calculation to be monotonic. The thickness of the standard foil was 2.5 cm and the thickness of samples mounted upon it was 1 cm. The fabrication of the layers of materials in the experimental assemblies was carefully monitored (for example, microirregularities on sample surfaces did not exceed 2.5 μm) and the sample density and thickness were measured with high precision.

The times of arrival of the shock fronts on the monitoring surfaces were determined by detecting light flashes radiation emitted by adjacent air which was transmitted to the photodetector by a light channel with polished internal

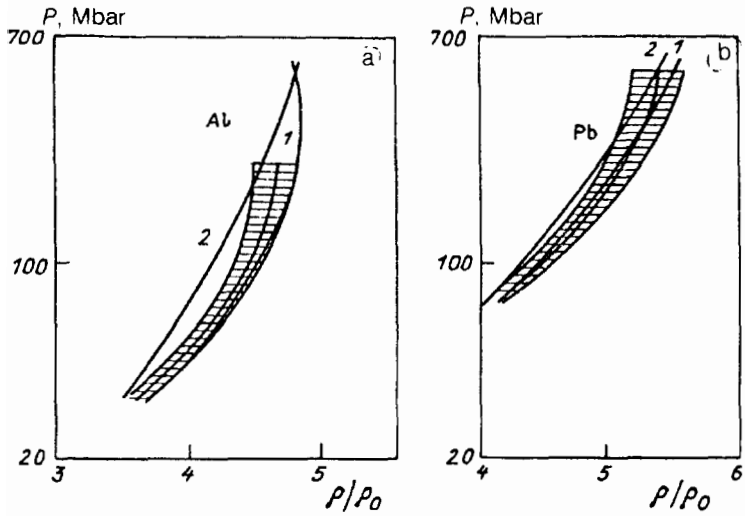

FIG. 17. Statistical analysis of experimental data for aluminum (a) and lead (b). Nominal position of shock adiabats—at the center of the corridor of uncertainty; *1*—calculated shock adiabats with interpolation,[53,90] *2*—TFQC.

metal walls. To ensure high measurement precision, the field of view of the photodetector contained three monitoring surfaces for the chosen pressure: one sample and two standard. Wave attenuation was determined experimentally by using two foils of the same composition. Mutual illumination by monitoring surfaces was prevented by inserting opaque barriers into the light channel. Each light channel contained two detectors and both recorded the complete signal. Because of the three-step shape of the signal, oscillographic recording was adopted as the preferred method. To increase the precision of measurement of the time intervals, the working signal was recorded on short sweeps after accurately known delays. The oscillograms were read and the data processed by modern computerized techniques. Measurements were made on the following pairs of materials: iron-aluminum, iron-lead, lead-iron, iron-water, and iron-quartzite. The first member in each pair was the first to be traversed by the wave.

The choice of the materials for investigation was dictated by the following considerations. Aluminum was interesting because it was relatively easy to produce pressures typical for the lower oscillation half-wave on its shock adiabat and the oscillation amplitude was large. Different theoretical models suggest that the oscillation amplitudes should decrease with increasing atomic number. Previous studies had indicated that lead should be chosen as the representative of high-Z media. Shell effects are nonmonotonic functions of Z. This means that, for chemical compounds containing atoms with different Z, the shell effects may cancel out for some values of ρ, T and mutually reinforce for other values. The corresponding calculations are much more laborious for complicated media than for simple ones. In view of the discussion given in Sec. 2, the unambiguous verification of a particular model capable of estimating shell effects is an even more acute problem in the case of complex materials. This explains the current interest in the shock compressibility of water and quartzite.

The average wave velocities on given surfaces were measured directly and their values on the contact boundaries were found from these results by calculation. The corrections for attenuation amounted to 2–8%, depending on the material (the largest corrections were obtained for lead). The inhomogeneous difference method[116] that locates the front of strong discontinuities and takes into account thermal conduction and adiabatic flow was used in the corresponding gas-dynamic computation program. The validity of the corrections was monitored experimentally. The main contribution to the uncertainty in wave velocity was due to the uncertainty in the choice of the point from which the recorded time was measured and was limited by the finite thickness of oscillograph beam.

The relationships deduced from different models for the above pairs of materials show that, in this particular pressure range, the maximum difference between the velocities lies in the range 1.4–3.4 km/s for the iron-aluminum pair and 1.2–2.3 km/s for the iron-lead pair, which exceeds the experimental uncertainty. Statistical analysis of the experimental data has enabled us to achieve an appreciable reduction in the uncertainty in the oscillation amplitude as compared with the uncertainty per point. Figure 17 shows the results of this analysis and clearly demonstrates the presence of shell-structure effects on the shock adiabats of aluminum and lead. The amplitudes are in good agreement with the predictions of the SCF model. The half-wave that was investigated seems to be compressed somewhat along the pressure axis as compared with calculations.

Plasma effects are particularly well defined in experiments[93] on compression by powerful shocks porous media with $m=\rho_0/\rho_{00}=3$ and 4. In these experiments, plasma with density of about ≈ 0.75 MJ/g, electron density $n_e \approx 2\times 10^{23}$ cm^{-3}, and pressures up to $P\approx 20$ Mbar (Fig. 18) was generated behind the shock front. At maximum temperatures $T\sim(3\text{–}5)\times 10^5$ K, the degeneracy of electrons ($n_e\lambda_e^3\approx 0.7$) is lifted in five-fold ionized plasma, and the Coulomb and short-term interactions remain strong ($\Gamma\approx 2$). It is clear from Fig. 18 that, under these conditions, the quasichemical model of plasma that includes the Coulomb interaction within the framework of the Debye ring approximation in the grand canonical ensemble of statistical mechanics[8] produces an acceptable description of dynamic experiment[117] whereas departures

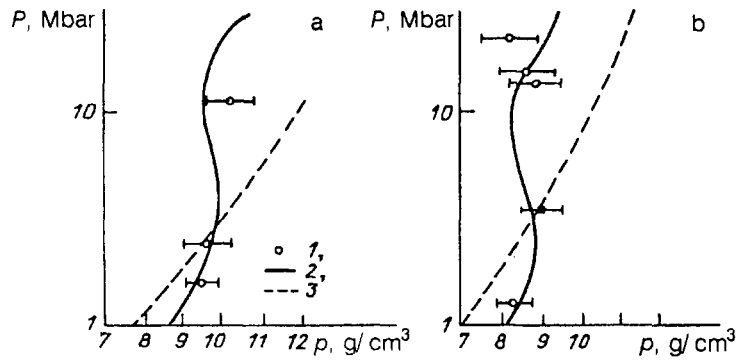

FIG. 18. Compression of porous copper by strong shock waves: a—$m=3.6$, b—$m=4$, *1*—experiment, *2*—bounded atom model, *3*—TFC calculation.

from the TFC model reach 20–30% in density and a factor between 1 and 10 in pressure.

Figure 19 shows a comparison between theoretical models and experimental data[11] at ultrahigh pressures.[118] At the record pressure value achieved in Ref. 110, i.e., $P=4$ Gbar, temperatures $T\approx 7\times 10^6$ K and energy densities of about 6×10^4 KJ/g, the plasma is fully ionized with $n_e\approx 3\times 10^{24}$ cm^{-3}, and is weakly degenerate ($\lambda_e^3 n_e\approx 0.06$). As the pressure is reduced, the nonideality parameter Γ rises on the shock adiabat from 0.05 to 8 (at $P\sim 10$ Mbar), and the short-range repulsion remains appreciable which justifies the utilization of the Debye ring approximation and the solid-sphere model (see Sec. 2; Refs. 8 and 117). It is clear (see Fig. 19) that the quasichemical plasma model and the cell models together provide a reasonable description of dynamic experiments down to the relatively low pressures of a few megabar. We note that, to solve the problem of the equation of state, there is probably little point in moving up pressure scale because the thermodynamic role of equilibrium radiation becomes increasingly important above the maximum pressures obtained in Ref. 110 (see dashed curve in Fig. 19).

Dynamic studies of the compressibility of chemical compounds have only just begun and it would be premature to attempt to draw any final conclusions. Calculations based on the model described in Ref. 48 have shown that water displays some manifestations of shell structure at pressures of the order of 100 Mbar, and that these effects are less well-defined in quartzite: the oxygen and silicon oscillations practically annul one another. Figure 20 illustrates the behavior of the oscillation amplitude throughout the range that is of interest in applications. The experimental data are not inconsistent with theoretical predictions. Further experiments with water are needed, and are now a feasible proposition, in the region in which the oscillations are particularly well defined.

When compared with earlier work, our measurements exhibit some special features. The steps that have been taken to produce well defined shock-front shapes in our experimental assemblies have resulted in somewhat greater corrections for attenuation, greater heating of the media, and a different method of extracting the data. Comparison with published information shows that all these new experimental results are in good agreement with the data in Ref. 107, 108, and 110, both at the lower and upper ends of the pressure range (see Ref. 124 for further details).

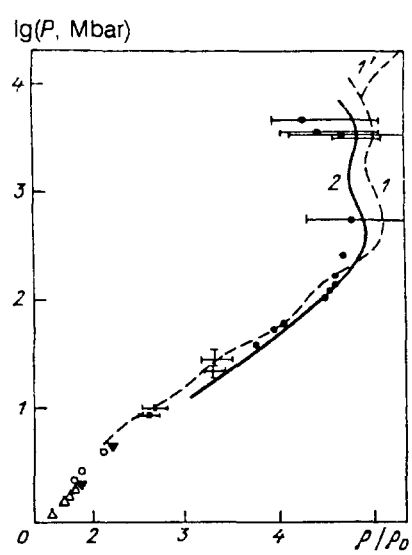

FIG. 19. Shock adiabat of aluminum: points—experiment, *1*—united-atom plasma model, *1'*—contribution of radiation, *2*—SCF calculation (for other models see Fig. 8).

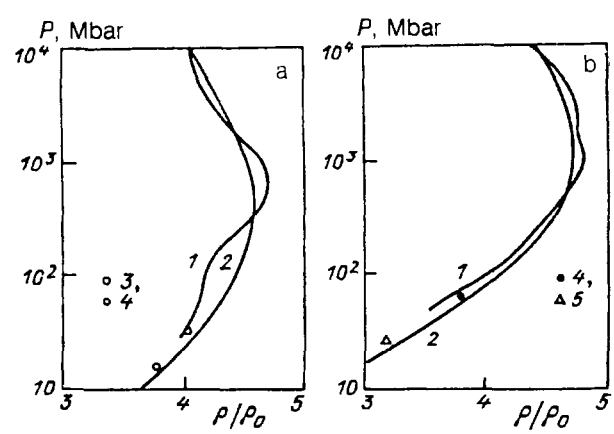

FIG. 20. Shell-structure effects on shock adiabats of water (a) and quartzite (b). *1*—SEOS (Ref. 48), *2*—TFQC: experimental results: *3*—Ref. 108, *4*—Ref. 124, *5*—Ref. 114.

6. ISENTROPIC EXPANSION OF SHOCK-COMPRESSED METALS

Powerful shock waves can be used produce high pressures and temperatures in shock-compressed media, but the region of reduced pressure that is occupied by the dense hot liquid and partially degnerate plasma is inaccessible to these techniques.[1,5,6] The situation can be remedied by using adiabatic expansion of condensed material after preliminary compression and heating by powerful shock waves.[1,3]

From the physical point of view there is particular interest in situations in which near- or post-critical states are produced in the rarefaction wave. The estimates of entropy performed in Ref 119 show that this requires sufficiently high shock intensities that lie at the limit of the range that can be achieved with chemical explosives. To reach the critical point in the rarefaction wave, the shock-wave amplitudes in continuous aluminum, copper, and tungsten must be aproximately 4.4, 7.5, and 16 Mbar, respectively.[119] Geometric and gradient cumulation techniques[76–80,87] are therefore used in experiments with rarefaction adiabats, as are methods of increasing irreversible energy dissipation that employ on porous targets.[69]

Expansion adiabats can be found experimentally by what is essentially a variant of the 'barrier' method.[1] A shock wave propagating in the material under investigation produces irreversible heating and compression up to the state A in Fig. 11. The emergence of the wave on the separation boundary on which there is a dynamically softer barrier results in a centered Riemann adiabatic expansion wave AB whereas a shock wave propagating with velocity D_B propagates in the barrier. By determining this velocity from the known target shock adiabat $T(u)$ we can find the pressure P_B and the mass velocity u_B in the barrier B, which are respectively equal to P and u for the adiabatically expanding target material.

By using barriers with different dynamic stiffness, and recording the corresponding P and u, we can determine the shape of the chosen isentrope between states on the shock adiabat at lower pressures. On the other hand, if we use shock-wave generators with different output power, and vary the initial porosity of the targets, we can vary the increase in shock entropy S and thus produce different isentropes covering the chosen region of the diagram of state. The thermodynamic parameters of the material are determined from hydrodynamic measurements of P, u by evaluating the Riemann integrals expressing the conservation laws for the particular self-similar flow:

$$V=V_A+\int_P^{P_A}\left(\frac{\mathrm{d}u}{\mathrm{d}P}\right)^2\mathrm{d}P,$$
$$E=E_A-\int_P^{P_A}P\left(\frac{\mathrm{d}u}{\mathrm{d}P}\right)^2\mathrm{d}P. \tag{6.1}$$

Mechanical measurements have now been augmented by optical temperature determinations through a transparent helium barrier.

In the experiments reported in Refs. 87 and 121, the 'soft' barriers consisted of materials with well-known shock adiabats, e.g., light metals (aluminum, manganese), Plexiglass, various ordinary and foam plastics of different porosity, and high pressure helium, argon, and xenon. For gaseous media, the shock adiabats were calculated from plasma models[8,12] whose validity was checked in an independent series of experiments.

The first experiments in which the rarefaction isentropes were determined[121] were performed with explosive planar shock generators employing aluminum and steel flyers with velocities of 5–6.5 km/s. Continuous and porous samples (grain size 10–15 μm) were placed in contact with aluminum, copper, or iron screens in which the impactors were brought to rest. The sample geometry (diameter 30 mm, height 2–3 mm) was such as to exclude lateral and rear rarefaction waves.

The velocity of the flyers and of the shocks in screens, targets, and 'light' barriers was measured by electrical-contact and optical-baseline methods. The electrical-contact sensors were copper pins with a diameter of about 0.5 mm, glued into channels with a diameter of about $\approx$0.8 mm and polished flush with the surface of each foil. To reduce stray inductances and to improve the signal shape, the pulse shaping circuits were placed on the experimental assembly. The electrical signals were recorded (to within $\lesssim$1 ns) by fast oscillographs (transmission bandwidth of measuring channels at least 1 GHz) with time markers common to all instruments applied at the same time. Each oscillograph received the output from six electrical-contact sensors placed so that the asynchronicity (slant) of the shock waves and their attenuation could be taken into account. The wave velocities in condensed media were measured by the electrical-contact method to within about 1%. The shock-wave velocity in the gas barriers was measured to within 1.5–2% by the optical baseline method, using a high-speed camera to record the beginning of plasma flash as the shock wave leaving the sample entered the gas, and the rapid increase in emission after its reflection from the transparent barrier placed in a known position.

Multistage cumulative ballistic systems[77,78,87] have been developed to increase the flyer velocity and, consequently, the shock-wave pressure. These devices rely on a mechanism analogous to the acceleration of a light body by elastic collison with a heavy body. These multistage ballistic systems were optimized by entropy and gas-dynamic calculations performed for the corresponding thermal and gas-dynamic processes with allowance for melting, evaporation, elastoplastic effects, and fracture.

These calculations and numerous experiments provided the basis for a number of two- and three-stage ballistic devices. In one of them, a steel flyer, 1 mm thick and 60 mm in diameter, was accelerated over a distance of 25 mm by detonation products to a velocity of 5 km/s. It was intercepted by a Plexiglass barrier 1 mm thick with a molybdenum impactor 0.1–0.2 mm thick and about 30 mm in diameter on the other side of the barrier. The impactor was thus accelerated over a distance of 2–3 mm to a velocity of 8.4 km/s, which was sufficient to produce a planar shock in a 10–12 mm diameter target. In the three-stage ballistic system, a steel impactor 2.5 mm thick was accelerated in

the first stage to 4.7 km/s and was the intercepted by a 5-mm layer of plastic explosive carrying a steel impactor 1 mm thick on the other side, which was thus accelerated to 6.7 km/s. In other respects, the three-stage device was the same as the two-stage generator.

The velocity of molybdenum impactors was extended in this way to 7–13 km/s as compared with the velocity of 5–6 km/s in the conventional end-point projection. The characteristic time intervals that have to be measured in these experiments amount to about 10^{-8} s which is shorter by an order of magnitude than the characteristic time intervals recorded in typical experiments with explosives.[3,6,9]

This is why, in the multistage systems, the shock compressibility and adiabatic expansion of continuous samples of aluminum, copper, bismuth, and titanium were determined by the optical baseline method, using stepped targets.[77,78,87] This was achieved by producing recesses of ~ 0.1 mm in the target material on the side of the incident impactor, with a Plexiglass window through which the observations were carried out mounted at a fixed distance from the target. Fast high-sensitivity electron-optic cameras (AGAT-SF) were used to measure the time intervals to within about 1.5–2% with a sweep rate of 2 ms/mn. It was thus possible in each experiment to obtain continuous and independent information on the approach of the impactor and on the entire flow field in the target whilst monitoring the one-dimensionality and stationarity of the field. The kinematic data was thus effectively was thus effectively extended by a factor of two.

This type of experiment has yielded the impact velocity W of the molybdenum flyer, the velocity of the shock wave in the target for different baselines, and the rate of adiabatic expansion of the metal into air at atmsopheric pressure. These parameters could then be used in the 'stopping' method[1] to calculate (with the help of the shock adiabat of molybdenum) the pressure P and the mass velocity u of the shock-compressed target and also the states on the rarefaction isentrope. Each experimental point was obtained by taking an average over 4–6 independent experiments.

Explosive conical Mach shock generators were used in the third series of experiments. They rely on geometric cumulation during irregular (Mach) reflection of a conically converging shock waves.[79,80,87] These devices produce additional concentration of energy as compared with planar geometry: the shock wave converges on the axis of symmetry and, at the same time, the stability of the flow is greater than for spherically converging shock waves. A two-dimensional numerical simulation using semiempirical equations of state[122] was carried out to find the optimum dimensions of the system and to estimate the stationarity and homogeneity of the flow. A typical shock-wave generator[80,87] consisted of a solid metal cone with an apex angle of 45° or 60° in which the shock wave was excited either directly by detonation products or by conical copper or aluminum liners, about ≈ 3 mm thick, accelerated by the detonation products to velocities of 3–4 km/s. The asynchronicity of the shocks along the cone generator was better than 50 ns. At a distance of about 40–50 mm from the apex of the copper cone, the Mach shock velocity was

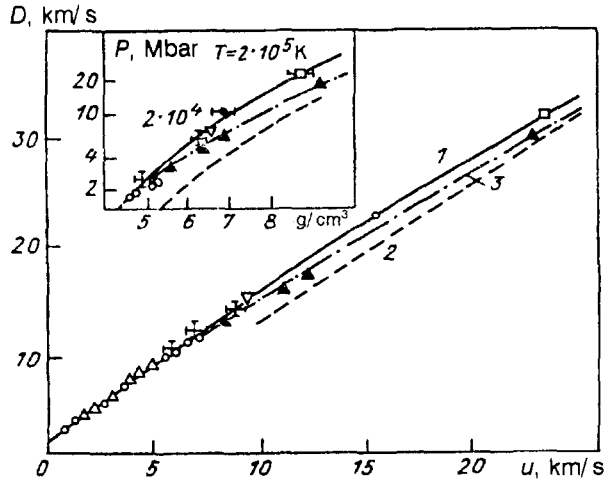

FIG. 21. Shock adiabat of aluminum: *1*—semiempirical equation of state,[12] *2*—TFC, *3*—interpolation between comparative measurements (quartzite as standard), points—experiment; insert shows the P, ρ plane.

about ≈ 12 km/s and the pressure was 5.7 Mbar.

As in the case of multistage systems, the kinematic parameters were determined by using stepped targets and optical recording of signals by fast electron-optical convertors. In several experiments, the radiation was conveyed from the targets to the photocathode of the electron-optical convertor by quartz lightguides.[123]

The shock-wave velocity in the copper cone (screen) could thus be determined in each experiment at different distances in the target, and a measurement could be made of its adiabatic expansion rate. Moreover, high-speed photography was used to monitor the curvature and attenuation of the shock waves. The other thermodynamic parameters could then be found by the reflection method with copper as the 'standard' material. When the rarefaction isentrope was determined, the shock-compressed bismuth and copper was allowed to expand in aluminum, Plexiglass, or air at atmospheric pressure. Each experimental point was obtained by averaging over 4–10 independent experiments with 2–4 recordings made for each. The precision of an individual measurement was estimated as 2–3% and the estimated average precision was about $\approx 1\%$.

Some of the experiments were performed with generators employing both geometric and gradient cumulation. In such cases, the conical Mach shock wave was allowed to interact via a condensed-explosive liner with a molybdenum (≈ 0.1 mm thick) or tungsten (≈ 0.25 mm thick) flyer which was thus acclerated over a baseline of 100–500 μm to a velocity of 15–16 km/s and then collided with a stepped copper target. The shock pressures achieved in these experiments were about ≈ 14 Mbar ($T \approx 5$ eV) and the entire isentropic expansion into air at atmospheric pressure was recorded. We note that these expansion parameters are in reasonable agreement with measurements reported by French scientists.[79]

Figure 21 shows the dynamic compression data obtained with the two-stage shock-wave generators for the

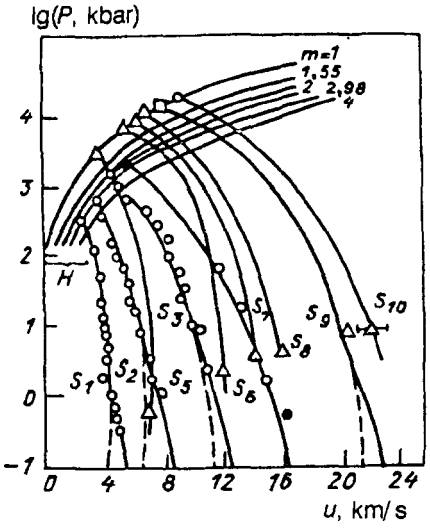

FIG. 22. P, u diagram of copper: H—shock adiabats with different initial porosity m, S—release adiabats; dashed curves—metastable curves, points—experiment.

degenerate plasma in aluminum[77,87] in the parameter range in which the experiments desscribed in Ref. 43 and the quantum-mechanical calculations reported in Ref. 125 predict a phase transition due to the rearrangement of electronic structure on compression. Our results contain no indication of any phase anomalies at low pressures, and are in agreement with data obtained with explosive and pneumatic shock-wave generators.[126] At ultrahigh pressures, they agree with the data obtained for strong explosions.

Figure 22 shows the P, u diagram for copper and Fig. 23 shows the corresponding diagram for bismuth.[87] In the latter case, calculations of thermodynamic parameters based on the Riemann integrals (6.1) show that the experiments were performed in a wide range lying between states on the shock adiabat with $P \approx 6.7$ Mbar, $\rho \approx 2.6\rho_0$ and the low-pressure metal vapor with $\rho \sim 10^{-2}\rho_0$.

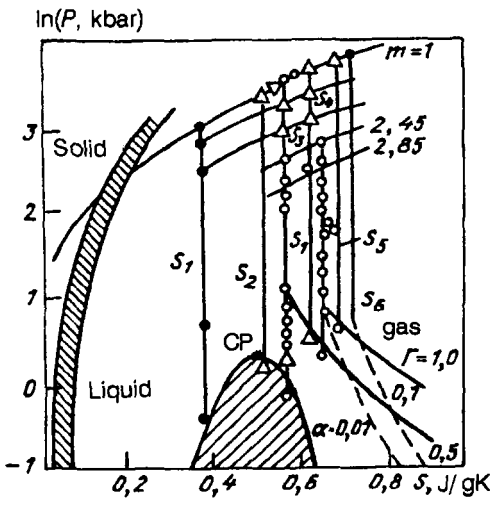

FIG. 23. Entropy diagram of bismuth: m—initial porosity on shock adiabats, S—release isentropes, α and Γ—ionization and non-ideality, CP—critical point; mixed-phase regions are shaded.

In this range of parameter values, adiabatic expansion of metals results in a complex range of physical processes that have not been adequately investigated. Degneracy is thus lifted, electrons recombine, the energy spectrum of the material undergoes a radical change, a metal-dielectric transition takes place in the electronically disordered structure, and the dense plasma produced in the process exhibits non-ideal properties for different forms of particle interaction.

There is particular interest in the strong expansion of metals, which takes them to the region of highly post-critical conditions. Figure 23 plots the nonideality parameter Γ and the degree of ionization $\alpha = n_e/(n_e + n_0)$, calculated from the chemical models of plasmas.[8] A similar analysis applied to copper shows that adiabatic expansion from states on the shock adiabat with $P \approx 14$ Mbar, $T \approx 5.2 \times 10^4$ K, and $V \approx 0.052$ cm^3/g leads to a weakly-ideal plasma with $P \approx 7.3$ kbar, $T \approx 9200$ K, $V \approx 1.3$ cm^3/g, $\Gamma \approx 1$, and $\alpha \approx 0.003$. This means that the entropy of a weakly-ionized metal vapor can be reliably calculated for such states from the quasi-ideal-gas approximation and, because the flow in the rarefaction wave is isentropic, the result is equal to the entropy of the highly-compressed metal.[1] This comparison with the semiempirical equation of state[12] produced reasonable agreement between them. It is clear that the results obtained with modern shock-wave generators have resulted for the first time in a unification of portions of the phase diagram corresponding to radically different physical states. Expansion isentropes join states of equal entropy in superdense degenerate plasmas on a shock adiabat with near- or post-critical states of weakly-ionized vapor and, in addition, as they enter the two-phase liquid-vapor region, they have energies and volumes that are in agreement with the parameters of the equilibrium curve. This has led to fruition Zel'dovich's idea[1,67] that it would possible to deduce a thermodynamically complete equation of state from the results of mechanical measurements. Because of the adiabatic condition, the entropy found for the rapidly expanding ideal vapor is found to be equal to the shock-compression entropy, and the equilibrium temperature of the shock-compressed material can then be calculated from the first law of thermodynamic.[127]

The experiments performed so far have revealed neither appreciable discontinuities in thermodynamic functions nor some other hydrodynamic anomalies that could be interpreted as plasma phase transitions (see Refs. 3 and 8 and the references therein). We emphasize that such phase transitions are particularly probable precisely in this part of the phase diagram because a rise in temperature and a reduction in the density of the Boltzmann plasma, and also an increase in pressure in the degenerate plasma (see Sec. 1) should lead to a relative reduction in the interaction between the particles.

Extreme stages in the expansion of the shock-compressed metals are accompanied by the entry of the isentropes into the two-phase liquid vapor region on the

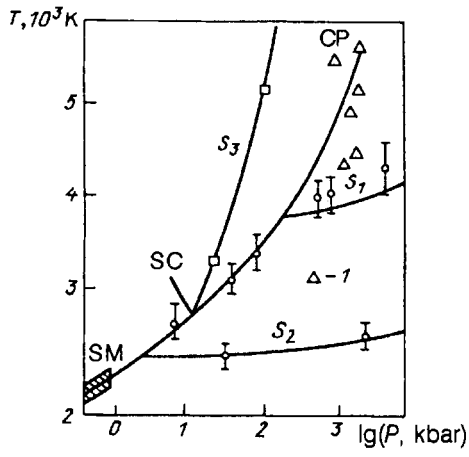

FIG. 24. Temperature measured in isentropic rarefaction waves S: SC—saturation curve, ST—static measurements, CP—critical point; *1*—estimates of the critical point parameters by different authors; other points—measured temperatures.

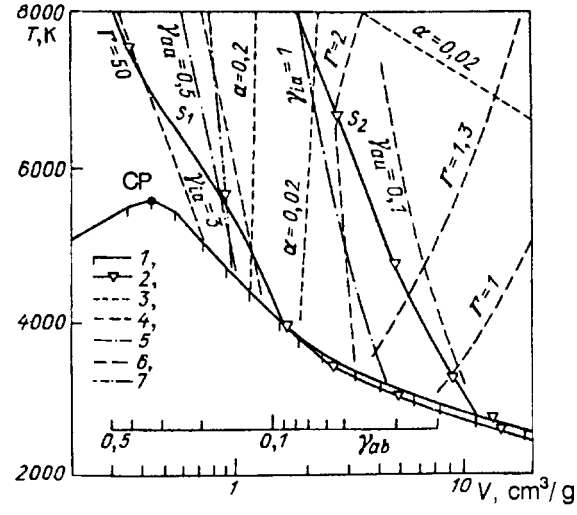

FIG. 25. The T, V diagram of bismuth: *1*—limit of two-phase region, *2*—S_1, S_2; *3*—α=const, *4*—Γ=const, *5*—γ_{ia}=const, *6*—$E_F/kT=1$.

liquid (evaporation) or vapor (condensation) side, which leads to a change in the slope of the isentropes (see dotted line in Fig. 22) and an additional increase in the rarefaction-wave velocity. This can be used to find the position of the boiling curve at high temperatures and pressures.

These kinematic measurements were augmented[128] in recent years by much more sensitive optical determinations of the brightness temperature of expanding lead. In these experiments, shock-compressed lead was allowed to expand into high-pressure helium which, because of its low molecular weight and high ionization potential, was not heated to any great extent by the shock waves and did not screen off the thermal radiation emitted by lead. Its optical emission was recorded by fast photodetectors (with a response of better than 0.1 ns), equipped with fiber-optic communication channels. Figure 24 shows the measured temperatures on isentropes entering the two-phase region, with an attendant sharp discontinuity on the $T(P)$ curve. Special experiments showed that the expansion of the metal to the same final pressure along different isentropes gave practically identical temperatures, which indicated that this was an equilibrium process. Nonequilibrium evaporation effects become appreciable on more extreme expansion stages (see Fig. 24).

The above experiments have given us the saturation curve for lead at pressures that were higher by more than an order of magnitude than the maximum pressures used in static measurements. They have located more precisely the position of the high-temperature part of this curve, which is particularly important for estimates of the overall form of the phase diagram and for the development of wide-range semiempirical equations of state.[12]

The detection of optical phenomena accompanying the arrival of powerful shock waves on the free surface provides interesting data on optical properties that are closely related to the structure, composition, and energy spectrum of expanding plasma.[1] The first experimental work on the emission of radiation by nonideal bismuth plasma when a powerful shock wave producing a pressure of a few million atmospheres emerged on the free surface was reported in Ref. 129. Powerful shock waves were generated by explosive cumulative propulsion devices in which thin (0.2 and 0.1 mm) molybdenum liners were accelerated to speeds of 7.0 and 8.3 km/s by using the gradient cumulation effect.[87] The impact of these liners on a bismuth target of 0.16 or 0.19 mm produced shock waves with amplitude pressure of 2.8 and 3.6 Mbar, respectively. The emergence of these shocks on the free surface of the sample was accompanied by the adiabatic expansion of the dense plasma whose optical emission was recorded by photodetectors (resolution about ≈ 10 ns at $\lambda = 700 \pm 5$ nm) whilst the plasma dynamics was recorded by fast electron-optic converters.

The nonideal plasma states produced in these experiments are shown in Fig. 25 on the T, V plane (T is the temperature and V is the volume). The figure shows the boundary of the two-phase region[139] (curve *1*) and also the isentropes $S_1(P_s=2.8$ Mbar) and $S_2(P_s=3.6$ Mbar) for particular segments identified experimentally. Curves of constant ionization $\alpha = n_e/m_i + n_a$. Coulomb nonideality $\Gamma = (8\pi n_e)^{1/2} e^3/(kT)^{3/2}$, and ion-atom interaction strength $\gamma_{ia} = (2\pi\alpha e^2 N)(r_a kT)^{-1} \approx 1[\alpha \approx 50 a_0^3]$ is the polarizability of neutrals and $r_a \approx 3a_0 = 3h^2/m_e(2\pi e)^2]$ were calculated from a plasma model that included degeneracy effects, the interaction between charges and between charges and neutrals, and also the atomic and ionic radii.[140] We see that the states detected in adiabatic rarefaction waves correspond to dense low-temperature plasma with a strong Coulomb interaction ($\Gamma \approx 1.3$–30), a change in the type of statistics near the $e_F/kT = (3n_e/\pi)^{2/3} h^2/8m_e kT = 1$ curve, and appreciable polarization interaction between charges and neutrals: $\gamma_{ia} = 0.5$–3. Since the states produced in the rarefaction wave are close to the boiling curve, the van der Waals interaction between neutrals is also significant, its parameters a and b being given by $\gamma_{aa} = Na/kT \approx 0.2$–1,

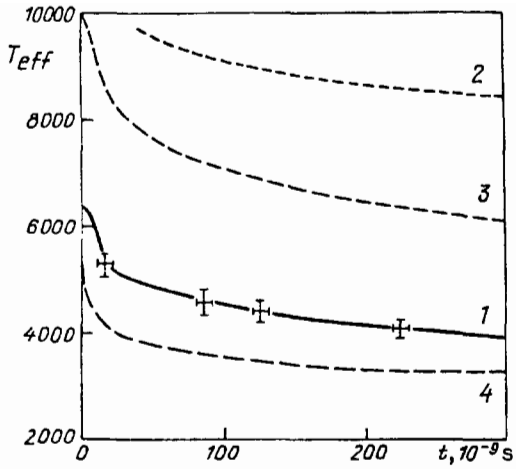

FIG. 26. The function $T_{eff}(t)$ on the surface of a rarefaction wave: *1*—experimental data (crosses indicate the ranges of uncetainty), *2*—Kramers–Unsold, *3*—calculations based on Ref. 140 including only the bremsstrahlung absorption channel, *4*—calculations based on Ref. 140 with the inclusion of bremsstrahlung and photoionization.

$\gamma_{ab}=3Nb\approx 0.03$–$0.3$ The optical radiation intensity leaving the expanding plasma is described by the simultaneous solution of the hydrodynamic and radiation transfer equations. The corresponding calculations are shown in Fig. 26 and confirm the estimates made in Ref. 1 according to which the effective layer of plasma that is responsible for the emission of radiation lies at a distance corresponding to unit optical path length to the interface with vacuum, i.e.,

$$\int_0^x k_\nu dx=1.$$

This condition enables us to estimate the magnitude of the plasma absorption coefficient k_ν from the semiempirical equation of state[139] and the measured function $T_{eff}(t)$. Since k_ν is an exceedingly rapidly-varying (exponential in T) function of the parameters of state, the temperature T_{eff} determined in this type of experiment is actually dictated by the local values of k_ν in the effective radiating layer.

The strong particle interaction illustrated in Fig. 1 complicates the systematic theoretical analysis of the composition and optical properties of the plasma and forces us to consider simplified methods. Curve *2* (Fig. 26) shows k_ν calculated from the Kramers–Unsold formula[8,133] with terms representing the photoionization of the upper excited states and bremsstrahlung in the field of ions and neutrals for a given degree of ionization of the plasma ($\alpha=1$). Curves *3* and *4* show the absorption coefficient calculated from a hydrogen-like model of the bismuth atom.[140] For low densities and low nonidealities S_2, detailed allowance for ionization processes results in reasonable agreement with experiment even for a very approxiamte description of the contribution of bremsstrahlung and photoionization processes to k_ν. The plasma density on the adiabat S_1 (Fig. 26) is greater by approximately an order of magnitude than S_2, which reduces the agreement between experiment and simple models and indicates that the contribution of photoionization processes is smaller in compressed plasma. It is possible that, as in Ref. 141, we are dealing here with a plasma transmission effect in which some of the high-lying energy levels are transferred to the continuum as the plasma density increases.

7. EXPERIMENTAL STUDY OF OPTICAL OPACITY AND THE INFLUENCE OF SHELL EFFECTS

At high energy densities in matter, e.g., in processes occuring in stellar interiors, energy transfer by electromagnetic radiation provides a significant contribution.[1] To describe such processes, we need to know the optical properties of compressed and highly heated materials. Phenomena in which there is local thermodynamic equilibrium between radiation and matter constitute an extensive class under these conditions. In many cases that are important in practice, all we need to know to describe the transfer of energy by radiation is the Rosseland opacity coefficient[1] $\varkappa$ which is a function of ρ and T. In general, $\varkappa(\rho,T)$ is a nonlinear function and the transfer of energy by electromagnetic radiation is analogous to nonlinear thermal conduction. Calculations of the opacity coefficient include terms representing Compton scattering, bremstrahlung by free electrons, and photoabsorption by bound electrons.[133] Difficulties are encountered when line absorption is calculated because it is then necessary to take into account a multitude of electronic configurations and all the possible transitions between them, as well as different broadening and splitting mechanisms such as the Stark effect, the Doppler effect, and so on.

The calculation of $\varkappa$ for given ρ and T is preceded by calculations of the ion wave functions, the population of electronic states, the self-consistent potential, the energy levels, the oscillation strengths, and so on.[134] The difficulties encountered in the theoretical description of matter that adequately takes into account the real properties of polyatomic systems in this particular range of density and temperature were discussed in Sec. 2. It is difficult to estimate the effect of the different simplifying assumptions used by the authors on calculated thermophysical characteristics, including the opacity coefficients. It is noted in Ref. 135 that there is a considerable difference between the values of $\varkappa$ obtained from first principles by different methods [all the required quantities are calculated from a given theoretical model; in Ref. 136 this is the Thomas–Fermi model and in Ref. 137 the modified Hartree–Fock–Slater model (Fig. 27)].

The difficult problem in calculating $\varkappa$ is how to allow for the different ionic states. This can be done rigorusly for low-Z media, but the statistical approach[138] has to be adopted for high-Z materials. This approach derives from the mean atom model, and the different ionic states are looked upon as fluctuations in the population around mean values. It is shown in Ref. 141 that these fluctuations modify the absorption spectrum and produce a 20% change in $\varkappa$ in this range of ρ and T. The problem that then arises, just as it does in thermodynamics, is the experimental verification of these methods. A theoretical approach, based essentially on statistical assumptions, is proposed in Ref. 143. The point is that the deceleration of ions and the

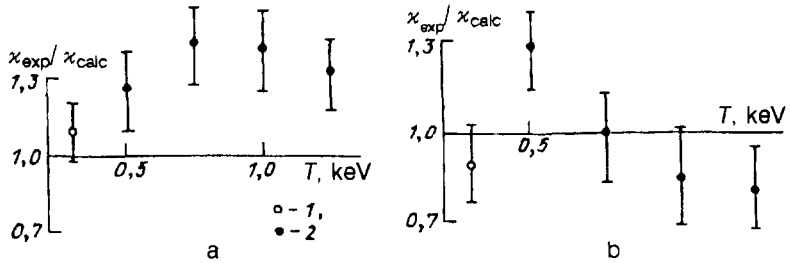

FIG. 27. Ratio of opacity coefficients obtained with the TF model:[136] a—aluminum, b—iron, *1*—experiment[135], *2*—experiment.[136]

absorption/emission of photons in matter are essentially determined by the same elementary processes, i.e., transitions between electronic energy levels. When the level separation is small, as it is for hot dense plasmas, the excitation spectrum can be described by the semiclassical approximation. This means that an adequate description of the ion and photon ranges in the material can be achieved within the frame-work of the same approach, the essence of which is as follows. The material is divided into elements in which the electron density may be assumed to be constant, but varies from one element to another. A physical variable characterizing the material as a whole is obtained by integrating over the local values. This approach is familiar from the cellular statistical Thomas–Fermi model and is used, for example, in calculations of the thermodynamic properties of materials.[4] The generalization of this simplified approach to the determination of ion and photon ranges in hot dense plasma has provided a basis for calculations of the range of fast particles and photons in dense plasmas.[143]

We have seen that studies of the properties of materials at high energy densities present a complex problem both from the standpoint of ensuring properly controlled conditions for the process and in respect of the measurement of physical parameters. One way of obtaining experimental data on opacity involves measuring the transmission of a sample of the material under investigation,[1] whose thickness is chosen so that the radiative heat transfer approximation can be used. Another possibility is based on a comparison of calculated and experimental transit times for thermal waves traversing particular samples. When a sufficiently high temperature is established on an inner boundary of the sample assembly, the energy transfer process initially occurs under the thermal wave regime (see for example, Ref. 1) but, after the thermal wave front has traversed a certain distance, it is overtaken by the shock discontinuity. At this stage, the flow of the medium may be approximately regarded as self-similar.[1] The time taken by the wave to cross the sample depends on its thickness and density, its opacity, its equation of state, and its temperature on its boundary. To determine the opacity ratio for different materials, we need only employ the same temperature source in all the measurements[135] (there is then no dependence on the uncertainty in T). The most accurate measurements in this approach are the relative measurements of $\varkappa$ in a pure material and in the same material containing small amounts of an impurity that does not affect the equation of state.

Absolute opacity measurements in this type of experiment involve the determination of temperature on the sample surface. The necessary precision of the measured temperature is ensured by recording the neutron spectrum from thermonuclear reactions in a solid mixture of deuterides or metal deuterides and tritides. The measuring assemblies containing such mixtures can be planar or centrally-symmetric layered systems[76] with a relatively higher energy cumulation level as compared with the preceding case.

Measurements of $\varkappa$ in systems in which the temperature distribution is determined by calculation are less accurate. They employ channels of a particular configuration, with walls made from different materials. The temperature conditions at entry to the channels are made as identical as possible. It is possible to ensure that the wave transit time in samples mounted on the channel walls is largely determined by the temperature on its surface and is very weakly dependent on the opacity on the wall material. This type of channel can be used for calibrating the procedures employed in temperature calculations. Other channels can then be used for experimental investigations of opacity. This was the approach that we have adopted in our studies. The equations of state verified in Ref. 124 were used to calculate wave arrival on monitoring surfaces. We must also mention experiments with laser heating of microspheres,[83] which were similar to our experiments but, in addition recorded, the propagation of thermal waves in metal targets. Table IV summarizes the results of our studies of aluminum and iron. It lists values of the ratio $\varkappa_{exp}/\varkappa_{calc}$ as a function of temperature[144] ($\varkappa_{calc}$ was calculated by the method described in Ref. 133 and 137). The uncertainty in these measurements was estimated as 15%. The first column of Table IV lists the results of our analysis of the measurements reported in Ref. 136. The values in parentheses show the calculated degree of ionization for a density of 1 g/cm^3.

TABLE IV.

Material	T, keV				
	0,25	0,5	0,75	1,0	1,25
Aluminum	1,08	1,26 (12,7)	1,44	1,41 (13,0)	1,32
Iron	0,89	1,31 (23,8)	1,0	0,85 (24,1)	0,81

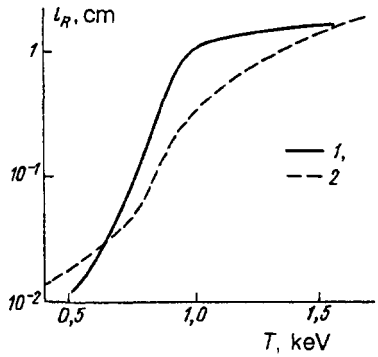

FIG. 28. Rosseland range of Al for $\rho = 1$ g/cm^3 as a function of temperature: *1*—local electron-density approximation[143], *2*—experimental data.

Calculations by the methods described in Refs. 136 and 137 show that the replacement of TF with MHFS as a means of calculating the self-consistent field leads to a 10–15% change in the opacity in this particular region, and the difference tends to oscillate in ρ and T. All this is confirmed expeimentally.

In aluminum at $T = 1$ keV, the main contribution to opacity is provided by the Compton effect, bremsstrahlung, and photoabsorption by hydrogen-like and helium-like ions that are present in small amounts. Line effects are small under these conditions. This is responsible for the reasonable agreement between experiment and theoretical values calculated in the mean-statistical approximation. Figure 28 illustrates the corresponding comparison with the results obtained in Ref. 143. The agreement is not as good at lower temperatures. Studies of the opacity of high-Z materials (e.g., gold) show that there is a discrepancy between theory and experiment by a factor of 2–3 even temperatures near 1 keV at which the target material contains a large amount of ionic configurations, the number of lines rises rapidly, there is a possibility that bands appear, and relativistic effects have to be taken into account. For materials such as gold, calculations based on the methods described in Ref. 136 show that a noticeable simplification occurs at temperatures of about 10 keV.

The calculated opacity coefficients are now more accurate following the inclusion of new effects (as compared with the method described in Ref. 137) and the verification of the validity of previouslyly adopted approximations. In the density and temperature ranges that are significant for many applied problems, good agreement is observed with the data in the SESAME library.[145]

Electronic shell-structure effects in the physical properties of highly compressed and heated media have been under active investigation for the last decade. The thermophysical characteristics of materials, the parameters describing the properties of targets for controlled thermonuclear fusion with inertical confinement, the calibrating relationships for measurements of the energy of nuclear explosions, and the general criteria for the stability of gas-dynamic flows have all been investigated.

Hydrodynamic analysis shows that the electronic shell structure has little effect on the characteristics of targets for controlled thermonuclear fusion with inertial confinement. For example, for a typical target, the calculated change in the focusing time and in energy release amounts to 0.5 and 5%, respectively.

Shell effects and the oscillations due to them in the thermophysical functions of hot compressed matter can lead to qualitative changes in hydrodynamic wave flows, e.g., to the loss of shock-wave stability. The stability of steady planar shocks in a medium with an arbitrary equation of state was first examined in Ref. 146 and, subsequently, in Ref. 147–151. It was shown that, depending on the slope of the shock adiabat, the stationary plane wave loses stability and splits into a series of shocks separated by continuous compression waves, or a more complicated flow sets in. Rarefaction shock waves can appear under these *conditions.*[1]

An analysis performed using the spline equation of state[155] has not revealed any anomalous segments due to shell effects on the shock adiabats[146] of aluminum, iron, molybdenum, lead, uranium, water, or quartzite in the region in which these adiabats oscillate. We note that the use of the semiempirical equation of state[152] of tungsten at the ultrahigh pressures at which degeneracy and nonideality are lifted has provided an indication of neutral instability[146] in the spontaneous emission of sound by shock waves.[153] A similar region has been found in nonideal cesium plasma[154] and in the vapor-gas region of copper in which these hydrodynamic anomalies are due to thermal-ionization and condensation effects.

CONCLUSION

We have attempted in this review to provide a systematic critical review of an extensive range of experimental data obtained in the last few years in the physics of extreme states. Experiments involving powerful underground explosions, which were being carried out until quite recently, have produced record thermal energy densities (10^9 J/cm^2) that were comparable with the specific energy release of nuclear explosives. The upper limit of the pressure range in 'hot' plasmas is now about 4 billion atmospheres, which is comparable with the pressures in the interior of the Sun and other stars. Above this limit, equilibrium radiation provides the dominant contribution, so that the thermodynamics of these exotic states is determined by radiation and is not very dependent on the structure of the material itself. The adiabatic expansion of a metal after it has been traversed by powerful shock waves takes it to a state that can be described as low-temperature nonideal plasma with a complex and extensive spectrum of particle interactions. It was precisely in this way that it has been possible to take normal metals to their near-critical state. This has yielded information about the high-temperature part of their boiling curves, the properties of boiling and condensation, and the radiative properties of nonideal plasmas.

It seems to us that these expensive and labor-intensive experiments are of considerable value to our understanding of the properties of matter at extreme energy densities that

produce a range of states that had always fascinated the penetrating intellect of our teacher Ya. B. Zel'dovich.

We believe that further advances in this part of physics will depend on the application of new experimental techniques for the concentration of energy, which will rely on powerful lasers, charged-particle beams, and electrodynamic accelerators. The aim of this paper has been to attract the attention of specialists to this interesting problem.

[1] Ya. B. Zel'dovich and Yu. P. Raĭzer, *The Physics of Shock Waves and High-Temperature Hydrodynamic Phenomena*, Academic Press, N.Y., 1967 [Russ. original, Nauka, M., 1966].
[2] Ya. B. Zel'dovich, *Chemical Physics and Hydrodynamics* [in Russian], Nauka, M., 1984.
[3] V. E. Fortov, Usp. Fiz. Nauk **138**, 361 (1982) [Sov. Phys. Usp. **25**, 781 (1982)].
[4] D. A. Kirzhnits, Yu. E. Lozovik, and G. V. Shpatakovskaya Usp. Fiz. Nauk **117**, 3 (1975) [Sov. Phys. Usp. **18**, 649 (1975)].
[5] D. A. Kirzhnits, Usp. Fiz. Nauk **119**, 357 (1976) [Sov. Phys. Usp. **19**, 530 (1976].
[6] L. V. Al'tshuler, Usp. Fiz. Nauk **85**, 197 (1965).
[7] M. Ross, Rep. Prog. Phys. **48**, 1 (1985).
[8] V. Fortov and I. Yakubov, *Physics of Nonideal Plasma*, Hemisphere, N.Y., 1990.
[9] L. Davison and R. A. Grahman, Phys. Rept., **55**, 255 (1979).
[10] G. I. Kanel' and V. E. Fortov, Usp. Mekh. No. 3, 3 (1987).
[11] E. N. Avrorin, B. K. Vodolaga, V. A. Simonenko, and V. E. Fortov, *Intense Shock Waves and Extreme States of Matter*, IVTAN, M., 1990.
[12] A. V. Bushman and V. E. Fortov, Usp. Fiz. Nauk **140**, 177 (1983) [Sov. Phys. Usp. **26**, 465 (1983)].
[13] R. M. More, VCRL Preprint, No. 94360 (1986).
[14] J. J. Duderstadt and G. A. Moses, *Inertial Confinement Fusion*, John Wiley, N.Y., 1982.
[15] A. F. Akkerman, A. V. Bushman *et al.*, Zh. Eksp. Teor. Fiz. **89**, 852 (1985) [Sov. Phys. JETP **62**, 489 (1985)].
[16] A. V. Bushman, O. Yu. Vorob'ev, *et al.*, *Numerical Modeling of the Effect of Intense Ion Beams on Metal Surfaces* [in Russian], OIKhF, Chernogolovka, 1987.
[17] G. Guderley, Luftfahrtforschung **19**, 302 (1942).
[18] E. I. Zababakhin and V. A. Simonenko, Prikl. Mat. Mekh. **29**, 334 (1965).
[19] E. I. Zababakhin and V. A. Simonenko, Prikl. Mat. Mekh. **42**, 573 (1978).
[20] J. D. Hansen and J. R. McDonald, *Theory of Simple Liquids*, Academic Press, N.Y., 1976.
[21] F. Ree, J. Phys. Chem, **87**, 2846 (1983).
[22] A. A. Abrikosov, L. P. Gor'kov, and I. E. Dzyaloshinskiĭ, *Methods of Quantum Field Theory in Statistical Physics*, Prentice-Hall, Englewood Cliffs, N.J., 1963 [Russ. original, Gostekhizdat, M., 1962].
[23] M. Baus and J. P. Hausen, Phys. Rept. **59**, 1 (1980).
[24] J. P. Hansen, *Strongly Coupled Plasma Physics*, edited by F. J. Rogers, Plenum, N.Y., 1986.
[25] V. K. Gryaznov and I. L. Iosilevskiĭ, Chisl. Metody Mekh. Sploshn. Sred **4**, 166 (1973).
[26] A. V. Bushman, B. N. Lomakin *et al.*, Zh. Eksp. Teor. Fiz. **69**, 1624 (1975) [Sov. Phys. JETP **42**, 828 (1975)].
[27] V. K. Bgryaznov, M. V. Zhernokletov *et al.*, Zh. Eksp. Teor. Fiz. **78**, 573 (1980) [Sov. Phys. JETP **51**, 288 (1980)].
[28] N. M. Tsidil'kovskiĭ, Usp. Fiz. Nauk **152**, 583 (1985) [Sov. Phys. Usp. **30**, 676 (1987)].
[29] D. Cepersely and B. Alder, Phys. Rev. Lett. **45**, 566 (1980).
[30] E. P. Wigner, Phys. Rev. **46**, 1002 (1934).
[31] V. K. Gryaznov *et al.*, *Thermophysical Properties of Working Media for Nuclear Gas Reactors* [in Russian], Atomizdat, M., 1980.
[32] W. J. Nellis *et al.*, Phys. Rev. Lett. **48**, 816 (1979); J. Chem. Phys. **73**, 6137 (1980).
[33] N. W. Ashcroft and N. D. Mermin, *Solid State Physics*, Holt, Rinehart, and Winston, N.Y., 1976.
[34] R. P. Feynman, N. Netropolis, and E. Teller, Phys. Rev. **99**, 1854 (1949).
[35] R. Latter, Phys. Rev. **99**, 1854 (1955).
[36] D. A. Kirzhnits, Zh. Eksp. Teor. Fiz. **62**, 2082 (1972) [Sov. Phys. JETP **35**, 1088 (1972)].
[37] D. A. Kirzhnits, Zh. Eksp. Teor. Fiz. **35**, 1545 (1959) [Sov. Phys. JETP **8**, 1081 (1959)].
[38] A. V. Bushman, V. E. Fortov, and I. I. Sharipdzhanov, Teplofiz. Vys. Temp. **15**, 1095 (1977).
[39] D. A. Kirznits and G. V. Shpatakovskaya, Zh. Eksp. Teor. Fiz. **62**, 2082 (1972) [Sov. Phys. JETP **35**, 1088 (1972)].
[40] G. V. Shpatakovskaya, Chisl. Metody Mekh. Sploshn. Sred **8**, 142 (1977).
[41] E. A. Kuz'menkov and G. V. Shpatakovskaya, Teplofiz. Vys. Temp. **27**, 677 (1989).
[42] A. I. Voropinov, G. M. Gandel'man, and V. G. Podval'nyĭ, Usp. Fiz. Nauk **100**, 193 (1970) [Sov. Phys. Usp. **13**, 56 (1970)].
[43] L. V. Al'tshuler and A. A. Bakanova, Usp. Fiz. Nauk **96**, 193 (1968) [Sov. Phys. Usp. **11**, 678 (1968)].
[44] O. V. Eroshin, Izv. Vyssh. Uchebn. Zav. Fiz. No. 4, 57 (1968).
[45] J. W. Zinc, Phys. Rev. **176**, 279 (1968).
[46] A. K. McMahan, M. T. Yin, and M. L. Cohen, Phys. Rev. **24**, 7210 (1986).
[47] B. F. Rozsnyai, Phys. Rev. A **5**, 1137 (1972).
[48] A. V. Andriyash and V. A. Simonenko, Vop. Atomn. Nauki Tekh., Ser. Teor. Prikl. Fiz. No. 2, 52 (1984).
[49] A. K. McMahan and M. Ross, Phys. Rev. **15**, 718 (1977).
[50] A. F. Nikiforov, V. G. Novikov, and V. B. Uvarov, Vop. Atomn. Nauki Tekh., Ser. Metod. Prog. Chisl. Resh. Zadach Mat. Fiz. No. 4, 16 (1979).
[51] A. Rosen and J. Lidgren Phys. Rev. **176**, 114 (1968).
[52] V. G. Novikov, IPM Preprint, No. 69, M., 1984.
[53] G. V. Sin'ko, Chisl. Metody Mekh. Sploshn. Sred **10**, 124 (1979).
[54] V. P. Kopyshev, Chisl. Metody Mekh. Sploshn. Sred **8**, 54 (1977).
[55] V. G. Novikov, IPM Preprint, No. 33, M., 1986.
[56] L. V. Al'tshuler, N. N. Kalitkin *et al.*, Zh. Eksp. Teor. Fiz. **77**, 1212 (1979) [Sov. Phys. JETP **50**, 613 (1979)].
[57] D. A. Young, J. K. Wolford *et al.*, Phys. Lett. **108A**, 157 (1985).
[58] F. J. Rogers, Phys. Rev. A **24**, 1531 (1981).
[59] D. A. Liberman, J. Quant. Spectros. Radiat. Transfer **27**, 335 (1982).
[60] P. Bridgman, *The Physics of High Pressure*, Bell and Sons, London, 1958.
[61] J. A. Xu, H. K. Mao, and P. M. Bell, Science, **232**, 1404 (1986).
[62] M. H. Rice, R. G. McQeen, and J. M. Walsh, Sol. State Phys. **6**, 1 (1958).
[63] W. J. Nellis, A. C. Mitchell *et al.*, J. Chem. Phys. **79**, 1480 (1983).
[64] W. J. Nellis, *High Pressure Measurement Techniques*, edited by G. N. Press, Applied Science Publishers, London, 1985, p. 68.
[65] P. S. Hawke *et al.*, Phys. Rev. Lett. **41**, 994 (1978).
[66] A. I. Pavlovskiĭ *et al.*, *Megagauss Technology and Pulsed Power Applications*, edited by C. M. Fowler, R. S. Caird, and D. J. Erickson, Plenum, N.Y., 1987.
[67] Ya. B. Zel'dovich, Zh. Eksp. Teor. Fiz. **32**, 1577 (1957) [Sov. Phys. JETP **5**, 1287 (1957)].
[68] S. B. Kormer *et al.*, Zh. Eksp. Teor. Fiz. **42**, 686 (1962) [Sov. Phys. JETP **15**, 477 (1962)].
[69] K. K. Krupnikov, M. I. Brazhnik, and V. P. Krupnikova, Zh. Eksp. Teor. Fiz. **42**, 675 (1962) [Sov. Phys. JETP **15**, 470 (1962)].
[70] M. Vau Thiel, J. M. Shaner, and E. Salinas, Lawrence Livermore Laboratory Report, 1977, VCRL-50-108, vols. 1–3.
[71] S. P. Marsh, LASL Shock Data, University of California Press, Berkely, 1980.
[72] L. V. Al'tshuler, S. B. Kormer *et al.*, Zh. Eksp. Teor. Fiz. **38**, 1061 (1960) [Sov. Phys. JETP **11**, 766 (1960)].
[73] L. V. Al'tshuler, *Shock Compression of Condensed Matter-91*, edited by S. Schmidt, R. Disk, J. Forbes, and D. Tasker, North-Holland, Amsterdam, 1992, p. 3.
[74] R. G. McQeen, J. M. Hapson, and J. N. Fritz, Rev. Sci. Instrum. **53**, 245 (1982).
[75] J. W. Shaner, J. M. Brawn, and R. G. McQeen, *High Pressure Science and Technology*, edited by C. Homa, R. MacCrone, and F. Whalley, Elsevier, Amsterdam, 1984, vol. 4, p. 137.
[76] E. I. Zababakhin, *Fifty Years of Mechanics in the USSR*, [in Russian], Nauka, M., 1970, vol. 2, p. 313.
[77] A. V. Bushman, I. K. Krasyuk, *et al.*, Pis'ma Zh. Eksp. Teor. Fiz. **39**, 341 (1984) [Pis'ma Zh. Eksp. Teor. Fiz. **39**, 411 (1984)].
[78] A. V. Bushman, B. L. Glushak *et al.*, Pis'ma Zh. Eksp. Teor. Fiz. **71**,

375 (1986) [Pis'ma Zh. Eksp. Teor. Fiz. **44**, 480 (1986)].
[79] P. Deaumont and A. Leygonie, *Proc. Fifth Symp. Detonation*, Pasadena, 1970, p. 430.
[80] O. V. Bazanov, V. E. Bespalov *et al.*, Teplofiz. Vys. Temp. **3**, 976 (1985).
[81] A. S. Mitchell and W. J. Nellis, Rev. Sci. Instrum. **52**, 347 (1981).
[82] J. C. Scidmore and E. Morris, *Thermodynamics of Nuclear Materials*, IAEA, Vienna, 1962, p. 173.
[83] S. I. Anisimov, A. M. Prokhorov, and V. E. Fortov, Usp. Fiz. Nauk **142**, 395 (1984).
[84] P. S. Hawke, Aerospace Eng. **1**, 110 (1983).
[85] M. M. Kondratenko *et al.*, Teplofiz. Vys. Temp. **25**, 159 (1988).
[86] L. V. Al'tshuler, A. A. Bakanova *et al.*, Zh. Prikl. Mat. Tekh. Fiz. No. 9, 3 (1981).
[87] B. L. Glushak, A. P. Zharkov *et al.*, Zh. Eksp. Teor. Fiz. **96**, 1301 (1989) [Sov. Phys. JETP **69**, 739 (1989)].
[88] W. H. Gust and E. B. Royce, Phys. Rev. B **8**, 3595 (1973).
[89] G. R. Gathers, J. Appl. Phys. **9**, 3291 (1986).
[90] A. T. Sapozhnikov and A. V. Pershina, Vop. Atomn. Nauki Tekh., Ser. Metod. Prog. Chisl. Resh. Zadach Mat. Fiz. No. 4, 47 (1979).
[91] V. F. Kuropatenko and I. S. Minaeva, Chisl. Metody Mekh. Sploshn. Sred **13**, 69 (1982).
[92] B. L. Rozhdestvenskiĭ and N. N. Yanenko, Chisl. Metody Mekh. Sploshn. Sred **13**, 69 (1978).
[93] V. N. Zubarev *et al.*, *Detonation* [in Russian], OIKhF, Chernogolovka, 1978.
[94] A. G. Ivanov and S. N. Novikov, Prib. Tekh. Eksper. 7, 135 (1963).
[95] A. V. Bushman, G. I. Kanel', A. L. Ni, and V. E. Fortov, *Intense Dynamic Loading of Condensed Matter*, Taylor and Francis, Washington DC, 1993 [Russ. original OIKhF, Chernogolovka, 1988].
[96] C. M. Barker and R. E. Hollenlach, J. Appl. Phys. **43**, 466 (1972).
[97] M. I. Belovolov, V. I. Vovchenko *et al.*, Zh. Tekh. Fiz. **1**, 27 (1988) [*sic*].
[98] Q. Johnson and A. C. Mitchell, *High Pressure Science Technology*, edited by B. Vodar and Ph. Marteau, Pergamon, Oxford, 1973.
[99] L. A. Egorov, E. V. Nitochkina *et al.*, Pis'ma Zh. Eksp. Teor. Fiz. **16**, 8 (1972) [JETP Lett. **16**, 4 (1972)].
[100] G. I. Kanel', E. B. Zaretskiĭ, P. A. Mogilevskiĭ, and V. E. Fortov, Dok. Akad. Nauk SSSR **316**, 111 (1991) [Sov. Phys. Dokl. **36**, 76 (1991)].
[101] S. B. Korner, Zh. Eksp. Teor. Fiz. **38**, (1968) [Sov. Phys. JETP **11**, 229 (1968)].
[102] V. E. Fortov and Yu. G. Krasnikov, Zh. Eksp. Teor. Fiz. **59**, 1645 (1970) [Sov. Phys. JETP **32**, 897 (1970)].
[103] B. Svendsen, J. D. Bass, and T. J. Ahrens, Phys. Rept. **180**, 3 (1990).
[104] C. E. Ragan III, M. G. Silberst, and B. C. Diven, J. Appl. Phys. **48**, 2860 (1977).
[105] L. P. Volokov, N. P. Voloshin *et al.*, Pis'ma Zh. Eksp. Teor. Fiz. **31**, 623 (1980) [JETP Lett. **31**, 588 (1980)].
[106] V. A. Simonenko, N. P. Voloshin *et al.*, Zh. Eksp. Teor. Fiz. **88**, 1452 (1985) [Sov. Phys. JETP **61**, 869 (1985)].
[107] L. V. Al'tshuler, B. N. Moiseev *et al.*, Zh. Eksp. Teor. Fiz. **54**, 785 (1968) [Sov. Phys. JETP **27**, 720 (1968)].
[108] R. F. Trunin, G. V. Simakov *et al.*, Zh. Eksp. Teor. Fiz. **62**, 1043 (1972) [Sov. Phys. JETP **35**, 550 (1972)].
[109] E. N. Avrorin, B. K. Vodolaga *et al.*, Pis'ma Zh. Eksp. Teor. Fiz. **31**, 727 (1980) [JETP Lett. **31**, 685 (1980)].
[110] A. S. Vladimirov and N. P. Voloshin, Pis'ma Zh. Eksp. Teor. Fiz. **39**, 69 (1984) [JETP Lett. **39**, 82 (1984)].
[111] I. Sh. Model', A. T. Narozhnyĭ *et al.*, Pis'ma Zh. Eksp. Teor. Fiz. **41**, 279 (1985) [JETP Lett. **41**, 332 (1985)].
[112] C. E. Ragan III, Phys. Rev. A **21**, 458 (1980).
[113] C. E. Ragan III, Phys. Rev. A **25**, 3360 (1982).
[114] C. E. Ragan III, Phys. Rev. A **29**, 1391 (1984).
[115] E. N. Avrorin, B. K. Vodolaga *et al.*, Pis'ma Zh. Eksp. Teor. Fiz. **43**, 241 (1986) [JETP Lett. 43, 308 (1986)].
[116] V. F. Kuropatenko, Chisl. Metody Mekh. Sploshn. Sred **15**, 81 (1984).
[117] V. K. Graznov, I. L. Iosilevskiĭ, and V. E. Fortov, Pis'ma Zh. Eksp. Teor. Fiz. **8**, 1378 (1982) [*sic*].
[118] V. K. Gryaznov and V. E. Fortov, Teplofiz. Vys. Temp. **25**, 1208 (1987).
[119] A. A. Leont'ev and V. E. Fortov, Prikl. Mekh. Tekh. Fiz. No. 3, 162 (1974).
[120] V. E. Fortov *et al.*, Pis'ma Zh. Eksp. Teor. Fiz. **20**, 20 (1974) [JETP Lett. **20**, 8 (1974)].
[121] L. V. Al'tshuler *et al.*, Zh. Eksp. Teor. Fiz. **78**, 741 (1980) [Sov. Phys. JETP **51**, 373 (1978)].
[122] A. V. Bushman, G. I. Korotkova *et al.*, Teplofiz. Vys. Temp. **23**, 1193 (1985).
[123] V. E. Bespalov, A. I. Vovchenko *et al.*, Pis'ma Zh. Tekh. Fiz. **12**, 3 (1986) [Sov. Tech. Phys. Lett.].
[124] E. N. Avrorin, B. K. Vodolaga *et al.*, Zh. Eksp. Teor. Fiz. **93**, 613 (1987) [Sov. Phys. JETP **66**, 347 (1987)].
[125] G. I. Gandel'man, Zh. Eksp. Teor. Fiz. **51**, 147 (1967) [Sov. Phys. JETP **24**, 99 (1967)].
[126] W. J. Nellis *et al.*, Phys. Rev. Lett. **60**, 1414 (1986); J. Appl. Phys. **69**, 2981 (1991).
[127] V. E. Fortov and A. N. Dremin, Fiz. Gor. Vzryva **9**, 743 (1973).
[128] V. G. Ageev *et al.*, Pis'ma Zh. Eksp. Teor. Fiz. **48**, 608 (1988) [Pis'ma Zh. Eksp. Teor. Fiz. **48**, 659 (1988)].
[129] S. V. Kvitov, A. V. Bushman *et al.*, Pis'ma Zh. Eksp. Teor. Fiz. **53**, 338 (1991) [Pis'ma Zh. Eksp. Teor. Fiz. **53**, 353 (1991)].
[130] M. V. Agranat, S. I. Anisimov, and B. I. Mokshantsev, Fiz. Tverd. Tela **29**, 3433 (1987) [Sov. Phys. Solid State **29**, 1966 (1987)].
[131] A. Ya. Polishchuk, *The Method of the Density Functional at Zero Temperatures and the Thermodynamics of Matter under Extreme Conditions* [in Russian], IVTAN Preprint No. 1-97, M., 1986.
[132] N. N. Kalitkin, L. V. Kuz'mina, and I. V. Ritus, *Quasi-ionic Interpolation of Thermodynamic Functions* [in Russian], IPM Preprint, No. 30, M., 1988.
[133] L. M. Biberman and G. E. Norman, Usp. Fiz. Nauk **91**, 193 (1967) [Sov. Phys. Usp. **10**, 52 (1967)].
[134] H. L. Meyer, J. Quant. Spectros. Radiat. Transfer **4**, 585 (1964).
[135] G. M. Eliseev, I. Sh. Model' *et al.*, Dok. Akad. Nauk SSSR **289**, 850 (1986) [Sov. Phys. Dokl. **31**, 635 (1986)].
[136] A. F. Nikiforov and V. B. Uvarov, Dok. Akad. Nauk SSSR **191**, 47 (1970) [Sov. Phys. Dokl. **15**, 191 (1970)].
[137] A. F. Nikiforov, V. G. Novikov, and V. B. Uvarov, Vop. Atomn. Nauki Tekh., Ser. Metod. Prog. Chisl. Resh. Zadach Mat. Fiz. No. 4, 27 (1979).
[138] V. V. Dragalov *et al.*, *Statistical Method of Allowing for Spectral Lines in Calculations of the Light Absorption Coefficient of Plasmas* [in Russian], IPM Preprint, No. 157, M., 1987.
[139] A. V. Bushman and V. E. Fortov, Sov. Tech. Rev. B, Thermal Phys. **1**, 219 (1987).
[140] W. Evelling *et al.*, *Thermophysical Properties of Hot Dense Plasma*, Treubner, Leipzig, 1990.
[141] V. E. Fortov, V. E. Bespalov *et al.*, *Strongly Coupled Plasma*, edited by S. Ichimaru, Elsevier, Amsterdam, 1990, p. 571.
[142] V. V. Dragalov and V. G. Novikov, IPM Preprint, No. 213, M., 1987.
[143] A. Ya. Polishchuk, V. E. Fortov, and V. S. Khloponin, Fiz. Plasmy **17**, 899 (1991) [Sov. J. Plasma Phys. **17**, 523 (1991)].
[144] B. K. Vodolaga, Proc. 12th AIRAPT and EHPRG Conf., Paderborn University, 1989, p. 819.
[145] SESAME 83, *Report on the Los Alamos Equation of State*, Library T4 Group, Los Alamos Nat. Lab. Report, NLAPL-83-4, Los Alamos NM, 1983.
[146] S. P. Dyakov, Zh. Eksp. Teor. Fiz. **27**, 288 (1954).
[147] V. M. Kantorovich, Zh. Eksp. Teor. Fiz. **33**, 1525 (1957) [Sov. Phys. JETP **5**, 1179 (1957)].
[148] G. W. Swan and G. R. Fowles, Phys. Fluids **18**, 28 (1975).
[149] N. M. Kuznetsov, Zh. Eksp. Teor. Fiz. **88**, 470 (1985) [Sov. Phys. JETP **61**, 275 (1985)].
[150] V. E. Fortov, Teplofiz. Vys. Temp. **10**, 168 (1972).
[151] A. L. Ni, S. G. Sugak, and V. E. Fortov, Teplofiz. Vys. Temp. **24**, 564 (1986).
[152] S. V. Bobrovskiĭ and V. M. Gogolev, Fiz. Gor. Vzryva No. 3, 594 (1967).
[153] T. N. Fortova, A. N. Dremin, and V. E. Fortov, Chisl. Metody Mekh. Sploshn. Sred **4**, 143 (1973).
[154] V. E. Fortov, Zh. Tekh. Fiz. **11**, 33 (1972) [*sic*].
[155] N. M. Barysheva, V. A. Zherebtsov, and G. V. Sin'ko, Vop. Atomn. Nauki Tekh., Ser. Metod. Prog. Chisl. Resh. Zadach Mat. Fiz. No. 2, 80 (1988).

Translated by S. Chomet